Report no. 03/17

Enhanced RFB method

Andrea Cangiani [a] Endre Süli

[a]The first author acknowledges the financial support of INdAM and EPSRC

The *residual-free bubble method* (RFB) is a parameter-free stable finite element method that has been successfully applied to solve a wide range of boundary–value problems exhibiting multiple-scale behaviour. If some local features of the solution are known a-priori, the approximation properties of the RFB finite element space can be improved by enriching it on selected edges of the partition by *edge–bubbles* that are supported on pairs of neighbouring elements (see [7]). Based on this idea, we define and analyse the *enhanced residual–free bubble* method for the solution of convection–dominated convection–diffusion problems in 2–D. Our a–priori analysis highlights the limitations of the RFB method and the improved global approximation properties of the new method. The theoretical results are supported by detailed numerical experiments.

Subject classifications: AMS(MOS): 65N30, 76M10, 76R50

Key words and phrases: convection-diffusion problems, residual-free bubbles

Oxford University Computing Laboratory
Numerical Analysis Group
Wolfson Building
Parks Road
Oxford, England OX1 3QD

April, 2004

Contents

1 Introduction

The underlying principle behind the use of *bubble methods* (see, e.g. [5]), is that of enriching the Galerkin finite element space with functions (bubbles) having compact support on every element of the given triangulation. The bubbles are successively eliminated through static-condensation, leaving a generalised Galerkin scheme for the original finite element space which is expected to have enhanced approximation properties. In general, we expect this to be the case when the numerical solution of the problem under consideration is sensitive to features present on scales that cannot be represented on the given mesh. For instance, in the framework of boundary–value problems for convection–dominated convection–diffusion equations, bubble methods have proved successful in capturing boundary layer behaviour, recovering many classical stabilised schemes [3].

The *residual-free bubble* method [9, 4] is defined by taking the bubble space as rich as possible; the resulting scheme then has the desirable property of being locally residual free, i.e. it is a solution to the partial differential equation under consideration inside every element.

Following [2], we note that a limitation of bubble methods in general, and of RFB in particular, is that only those subgrid features can be modelled that do not cross the inter-element boundaries. We propose to further enrich the RFB method with *edge-bubbles*, i.e. bubbles with compact support on pairs of elements. The number of such edge-bubbles should be small relative to the total number of degrees of freedom, the idea being that they should be introduced only on those edges where it is crucial that the subgrid scales are captured.

We show through a-priori analysis, and illustrate by numerical experiments, that the resulting procedure, the *enhanced residual-free bubble method* (RFBe), can be successfully applied to improve the RFB resolution of boundary layers in convection-dominated convection-diffusion problems. A crucial property of the method is that the locally introduced edge-bubbles give global improvement of the solution, showing that they have a stabilising effect on the scheme. Moreover, the RFBe numerical solution is able to capture the correct behaviour inside boundary layers.

We present the method in Section 2, applying the general framework for multilevel methods proposed by Brezzi & Marini in [7]. In Section 3, we explain how the edge-bubbles are defined for convection-dominated convection-diffusion problems. Our choice is justified in Section 3.1 through a-priori analysis. Finally, Section 4 is dedicated to the fully discrete version of the method (i.e. including the numerical approximation of the bubbles). The theoretical results are confirmed by numerical experiments.

2 The RFBe method

Given a bounded polygonal domain Ω in $\mathbb{R}^2$, let $\mathcal{L}(\cdot,\cdot)$ be a bounded coercive bilinear functional on $V = H_0^1(\Omega)$ and let $f \in L^2(\Omega)$. We consider the elliptic boundary value problem in variational form:

$$\begin{cases} \text{find } u \in V \text{ such that} \\ \mathcal{L}(u,v) = (f,v) \qquad \forall v \in V. \end{cases} \tag{2.1}$$

Assume that we are given a shape-regular triangulation $\mathcal{T}$ of Ω such that any $T \in \mathcal{T}$ is affine-equivalent to a reference element $\widehat{T}$ through an affine map F_T. Moreover, assume that the intersection of the closure of any two elements is either the empty set, a common vertex or an entire edge. Finally, let h be the triangulation parameter, i.e. the maximum elemental diameter.

We define over $\mathcal{T}$ the standard finite element space V_h of all piecewise linear functions (if $\widehat{T}$ is a triangle) or piecewise bilinear functions (if $\widehat{T}$ is a rectangle). Moreover, let B_h be the space of residual-free bubbles, i.e. the set of all functions in V that have compact support on every element $T \in \mathcal{T}$. That is, we define

$$V_h = \left\{ v_h \in H_0^1(\Omega) : w_{h|_T} \in \mathcal{P}_1(T) \ (\text{or } w_{h|_T} \circ F_T \in \mathcal{Q}_1(\widehat{T})) \quad \forall T \in \mathcal{T} \right\}, \tag{2.2}$$

$$B_h = \bigoplus_{T \in \mathcal{T}} H_0^1(T). \tag{2.3}$$

The *residual-free bubble* finite element space is then defined as $V_{RFB} = V_h \oplus B_h$, the direct sum being ensured since V_h does not contain nontrivial bubbles, i.e. $V_h \cap B_h = \{0\}$.

We mention here that it is possible to define higher-order residual-free bubble finite element spaces, the general recipe being that the bubble space should be as large as possible, as explained by Brezzi in [2].

The residual-free bubble method (RFB) is given by restricting (2.1) to the subspace V_{RFB}:

$$\begin{cases} \text{find } u_{RFB} \in V_{RFB} \text{ such that} \\ \mathcal{L}(u_{RFB},v) = (f,v) \qquad \forall v \in V_{RFB}. \end{cases} \tag{2.4}$$

Thanks to the richness of the space of bubbles B_h, the solution u_{RFB} has the desirable property of being residual-free on the interior of any element (see [8]).

As we shall see later, the bubble part of the solution can be eliminated, at least formally, from the RFB formulation through a static condensation procedure which leads to a generalised Galerkin formulation over the standard finite element space V_h. In other words, the RFB method can be formulated as a two-level algorithm which corresponds to a sort of divide–and–conquer principle: the space of bubbles B_h should take into account the fine scales of the problem while the solution on V_h gives an approximation of the global behaviour of u.

The draw-back of such a two-level procedure is that only the small scales that do not cross the boundary of any element of the triangulation will be taken into account.

Following an idea by Brezzi [2], we propose to further enrich the RFB space with the aim of improving the approximation properties on the skeleton of the triangulation.

The framework is that of the general augmented space method proposed by Brezzi and Marini in [7], which is defined as follows.

Let Σ be the the skeleton of our partition $\mathcal{T}$, i.e. the union of the boundaries of all elements in $\mathcal{T}$, and let Φ be the space of traces of V on Σ.

An *augmented subspace* is defined by considering all the extensions onto $\overline{\Omega}$ from a finite-dimensional subspace of Φ. That is, given a subspace $\Phi_H \subset \Phi$ of finite dimension, we define the space

$$V_a := \left\{ v \in V \,:\, v_{|\Sigma} \in \Phi_H \right\}.$$

The augmented space formulation is obtained by restricting (2.1) to V_a:

$$\begin{cases} \text{find } u_a \in V_a \text{ such that} \\ \mathcal{L}(u_a, v_a) = (f, v_a) \qquad \forall v_a \in V_a. \end{cases} \tag{2.5}$$

Existence and uniqueness are ensured by the coercivity of the bilinear form $\mathcal{L}$.

By definition, the augmented space V_a always contains as a subspace the residual-free bubble space B_h as defined in (2.3). The RFB method is obtained from the above general formulation simply by choosing Φ_h as the space spanned by the traces of V_h.

We can also identify a second subspace V_l, which depends on the bilinear form $\mathcal{L}$:

$$V_l := \{ v_l \in V_a \,:\, \mathcal{L}(v_l, v_b) = 0 \quad \forall v_b \in B_h \}, \tag{2.6}$$

and observe that we have the splitting

$$V_a = V_l \oplus B_h. \tag{2.7}$$

In the special case in which V_a is equal to V_{RFB}, we also have, by definition,

$$V_a = V_{RFB} = V_h \oplus B_h.$$

Since V_h and V_l are not equal, the two characterisations of the RFB space are different. Thus, the augmented space formulation naturally gives a new interpretation to the RFB method. Indeed, the solution u_a of (2.5) can be characterised as follows (see [7]).

Theorem 2.1 *Let u_a be the unique solution of (2.5). Then, its decomposition according to (2.7) is given by $u_a = u_l + u_b^f$ where u_b^f is the unique solution in B_h of*

$$\mathcal{L}(u_b^f, v_b) = (f, v_b) \qquad \forall v_b \in B_h, \tag{2.8}$$

and u_l can be characterised as the unique solution in V_l of

$$\mathcal{L}(u_l, v_l) + \mathcal{L}(u_b^f, v_l) = (f, v_l) \qquad \forall v_l \in V_l. \tag{2.9}$$

Proof. The existence of unique solutions to problems (2.8) and (2.9) is ensured by the coercivity of $\mathcal{L}$. Let $u_a = u_l + u_b$ be the unique decomposition of u_a according to (2.7). Testing in (2.5) with $v_a = v_b \in B_h$ and using the definition (2.6) we have

$$(f, v_b) = \mathcal{L}(u_a, v_b) = \mathcal{L}(u_l, v_b) + \mathcal{L}(u_b, v_b) = \mathcal{L}(u_b, v_b),$$

that is, $u_b = u_b^f$. Finally, testing in (2.5) with $v_a = v_l \in V_l$, we see that u_l satisfies (2.9). □

Remark. The *bubble equation* (2.8), i.e. the equation obtained from the augmented space formulation by testing in the bubble space, has the appealing property of being independent of u_l. Moreover the two equations (2.8) and (2.9) decouple if $\mathcal{L}$ is a symmetric (bilinear) functional, since in this case $\mathcal{L}(u_b^f, v_l) = \mathcal{L}(v_l, u_b^f) = 0$ by (2.6).

We now come to the definition of our algorithm. Assume that a (small) number of internal edges $\Gamma_j, j = 1, \ldots, N_e$, have been identified as requiring some extra resolution.

The idea involves defining N_e (or possibly more) new basis functions, each of which is related to one of the edges identified. That is, we consider as space of traces Φ_h the traces of V_h supplemented by a relatively low-dimensional space of *edge-bubbles* each of which has support on the two elements which share a particular edge. The definition of such new edge–bubbles will be dependent on the problem under consideration; indeed the edge–bubbles may be chosen by exploiting the differential equation or, alternatively, some information about the solution obtained through a previous computation.

To summarise, if $T_j^{\pm}$ are the two elements sharing the edge Γ_j, we define the edge-bubble $e_j \in H_0^1(\Omega)$ as follows:

- the support of e_j is contained in $\overline{T}_j^+ \cup \overline{T}_j^-$;
- the value of e_j on $\Gamma_j = \overline{T}_j^+ \cap \overline{T}_j^-$ is chosen to have some particular feature; e.g. it is the solution of a nonhomogeneous boundary value problem on Γ_j subject to homogeneous boundary conditions on $\partial\Gamma_j$;
- inside $T_j^{\pm}$, e_j is required to be the solution of

$$\mathcal{L}_{T_j^{\pm}}(e_j, v) = 0 \qquad \forall v \in H_0^1(T_j^{\pm}), \tag{2.10}$$

  where $\mathcal{L}_{T_j^{\pm}}$ is the restriction of $\mathcal{L}$ to $T_j^{\pm}$.

The augmented space formulation now follows, as we have said, by defining Φ_h as the sum of the space of traces of V_h and the space spanned by the edge-bubbles.

Alternatively, in order to take advantage of the well-known approximation properties of the subjacent finite element space V_h, we can define our method as an enrichment of RFB as follows.
We observe that the space of edge-bubbles

$$E_h := \operatorname{span}\{e_j, j = 1, \ldots, N_e\},$$

is clearly in direct sum with B_h and also with V_h since $e_{j_{|\Gamma_j}}$ can be seen as a (nontrivial) one-dimensional bubble over Γ_j.

Thus, as already discussed in the case of the RFB method, we have the following alternative splitting of the augmented space:

$$V_a = V_h \oplus E_h \oplus B_h =: V_P \oplus B_h. \tag{2.11}$$

Since in (2.11) we have a direct sum, every $v_a \in V_a$ can be uniquely decomposed as a sum over the three subspaces. Hence, the RFBe formulation reads

$$\begin{cases} \text{find } u_a = u_h + u_e + u_b \in V_a = V_h \oplus E_h \oplus B_h \text{ such that} \\ \mathcal{L}(u_h + u_e + u_b, v_a) = (f, v_a) \qquad \forall v_a \in V_a. \end{cases} \tag{2.12}$$

As before, testing in (2.12) with $v_b \in B_h$, we obtain the bubble equation

$$\mathcal{L}(u_b, v_b) = (f, v_b) - \mathcal{L}(u_h, v_b) \qquad \forall v_b \in B_h, \tag{2.13}$$

where we have used the 'orthogonality' of E_h and B_h with respect to $\mathcal{L}$ expressed by (2.10). Starting from the standard RFB method formulation (2.4), we would obtain exactly the same bubble equation. That is to say, the introduction of the edge-bubbles leaves the static condensation procedure unchanged.

Formally, static condensation is carried out as follows. Letting φ_j, $j = 1, \ldots, N_T$, be the local basis functions for V_h on a generic element $T \in \mathcal{T}$ and considering the local decomposition $u_{h|_T} = \sum_{j=1}^{N_T} U_j \varphi_j$, we have from (2.13):

$$u_{b|_T} = \sum_{j=1}^{N_T} U_j b_j + b_f, \tag{2.14}$$

where

$$\begin{cases} b_j \in H_0^1(T) \text{ such that} \\ \mathcal{L}(b_j, v) = -\mathcal{L}(\varphi_j, v) \qquad \forall v \in H_0^1(T), \end{cases} \tag{2.15}$$

and

$$\begin{cases} b_f \in H_0^1(T) \text{ such that} \\ \mathcal{L}(b_f, v) = (f, v) \qquad \forall v \in H_0^1(T). \end{cases} \tag{2.16}$$

Assume that the variational problems (2.15) and (2.16) have been solved. Testing in (2.12) with $v \in V_P$ and substituting u_b using (2.14), we arrive at the following problem on the space V_P:

$$\begin{cases} \text{find } u_h + u_e \in V_P \text{ such that} \\ \\ \mathcal{L}(u_h + u_e, v) + \displaystyle\sum_{T \in \mathcal{T}} \left(\sum_{j=1}^{N_T} U_j \mathcal{L}_T(b_j, v) \right) = (f, v) - \sum_{T \in \mathcal{T}} \mathcal{L}_T(b_f, v) \qquad \forall v \in V_P. \end{cases} \tag{2.17}$$

Thus, as for the standard RFB method, the RFBe method results in a generalised Galerkin formulation except that this generalised Galerkin formulation is now over the locally augmented finite element space $V_P = V_h \oplus E_h$.

So far, the discussion was concerned with the general formulation (2.1). On the other hand, the construction and the analysis of the method are clearly problem-dependent. In the next section we present an example of a successful application of RFBe and show how an a-priori error analysis can be used to determine a suitable choice of edge-bubbles.

3 Increasing the resolution of boundary layers

We exemplify edge-bubbles designed to capture boundary layer behaviour and we prove, through a-priori error analysis, that the particular choice of edge-bubbles results in reduction of the discretisation error beyond that of the classical RFB method.

Consider the following boundary value problem for the convection-diffusion equation:

$$\begin{cases} Lu := -\varepsilon \Delta u + \boldsymbol{a} \cdot \nabla u = f & \text{in } \Omega = (0,1)^2, \\ u = 0 & \text{on } \partial\Omega, \end{cases} \tag{3.1}$$

where the convection field $\boldsymbol{a}$ is assumed continuously differentiable. In the convection-dominated regime, the solution exhibits a normal boundary layer on parts of $\partial\Omega$ where $\boldsymbol{a} \cdot \boldsymbol{n} > 0$, with $\boldsymbol{n}$ denoting the unit outward normal vector to $\partial\Omega$. This part of $\partial\Omega$ will be referred to as the outflow boundary. It is in the vicinity of the outflow boundary, in particular, that we aim to obtain increased accuracy over a standard Galerkin finite element method and over RFB by careful selection of edge-bubbles.

In order to do so, we use information about the behaviour of the solution based on performing an asymptotic analysis, in much the same way as in [12].

We note that the availability of an asymptotic expansion of the analytical solution u in terms of the small parameter ε is only required for analytical purposes and is not needed in the practical implementation of the method.

To fix ideas, we assume that

$$\boldsymbol{a} = (a_1, a_2), \qquad \text{where } a_1, a_2 \geq c_a > 0,$$

so that the outflow boundary $\partial\Omega_+$ coincides with the union of the two sides $x = 1$ and $y = 1$. The analysis below is valid as long as internal layers are absent. For this purpose, we assume that f is a smooth, say, $f \in W^1_\infty(\Omega)$. Finally, we assume that $\operatorname{div} \boldsymbol{a} \leq 0$ in Ω to ensure coercivity of the bilinear functional associated with L. Under the above hypothesis, the boundary value problem (3.1) admits a unique weak solution $u \in H^1_0(\Omega)$.

The reduced problem (corresponding to $\varepsilon = 0$) is defined by

$$\begin{cases} \boldsymbol{a} \cdot \nabla u_0 = f & \text{in } \Omega, \\ u_0|_{x=0} = u_0|_{y=0} = 0, \end{cases} \tag{3.2}$$

with solution $u_0 \in W^1_\infty(\Omega)$ since first-order partial derivatives of u_0 exhibits discontinuities across the characteristic passing through the inflow corner $(0,0)$ of Ω. The asymptotic approximation of u to first order is

$$\begin{aligned} u_{\rm as}(x,y) = & u_0(x,y) - u_0(1,y)\mathrm{e}^{-a_1(1,y)\frac{1-x}{\varepsilon}} - u_0(x,1)\mathrm{e}^{-a_2(x,1)\frac{1-y}{\varepsilon}} \\ & + u_0(1,1)\mathrm{e}^{-a_1(1,1)\frac{1-x}{\varepsilon}}\mathrm{e}^{-a_2(1,1)\frac{1-y}{\varepsilon}} \equiv u_0(x,y) + u_c(x,y), \end{aligned} \tag{3.3}$$

where the last term is the *corner layer* correction, relevant in the vicinity of $(1,1)$ where the two boundary layers intersect (see, e.g. [10]).

The accuracy of the asymptotic approximation $u_{\rm as}$ depends on the smoothness of the reduced solution. For the problem under consideration, for which $u \in H^1_0(\Omega)$ and $u_0 \in W^1_\infty(\Omega)$, it has been proven by Schieweck ([18], Lemma 4.4, pp. 33; see also [15], pp. 184) that:

$$\varepsilon |u - u_{\rm as}|^2_{1,\Omega} + ||u - u_{\rm as}||^2_{0,\Omega} \leq C\varepsilon, \tag{3.4}$$

where C is a constant independent of ε.

We now turn to the definition of the RFBe method. Let $\mathcal{T}$ be a shape-regular axiparallel rectangular partition of $\overline{\Omega}$. Thus, the mesh is the tensor-product of the subdivisions $0 = x_0 < x_1 < \cdots < x_m = 1$ and $0 = y_0 < y_1 < \cdots < y_n = 1$.

Assume that the boundary layer is not resolved by the given mesh. We propose to introduce edge-bubbles on those edges that cross the boundary layer. The number of such edges is $m + n - 2$ which in turn is bounded byKh^{-1} where h is the maximum element diameter and K is a constant depending only on the shape–regularity of the mesh.

Let us introduce the following pieces of notation. We define as *boundary layer region* a neighbourhood of the outflow boundary of width

$$\kappa = \varepsilon \ln(1/\varepsilon), \tag{3.5}$$

in the direction orthogonal to the boundary (see Figure 1). Then, we denote by $\Omega_{\rm bl}$ the union of all elements that intersect the boundary layer region and by $\Omega_{\rm out}$ the union of all of the remaining elements. The partition of Ω into $\Omega_{\rm bl}$ and $\Omega_{\rm out}$ induces two subpartitions $\mathcal{T}_{\rm bl}$ and $\mathcal{T}_{\rm out}$ of $\mathcal{T}$. Similarly, let $\Gamma_{\rm bl}$ be the set of all edges that intersect the boundary layer region, $\Gamma_{\rm out}$ the set of all the remaining edges. Finally, given an edge Γ we let $h_\Gamma := |\Gamma|$.

We define an edge bubble only on edges which belong to $\Gamma_{\rm bl}$. Notice that only the value of the edge-bubble on the edge itself is left free by the definition given in Section 2.

On every $\Gamma \in \Gamma_{\rm bl}$ we define the edge-bubble e on Γ as the solution of the one-dimensional boundary value problem

$$\begin{cases} L_\Gamma e_\Gamma = 1 & \text{in } \Gamma \\ e_\Gamma = 0 & \text{on } \partial\Gamma, \end{cases} \tag{3.6}$$

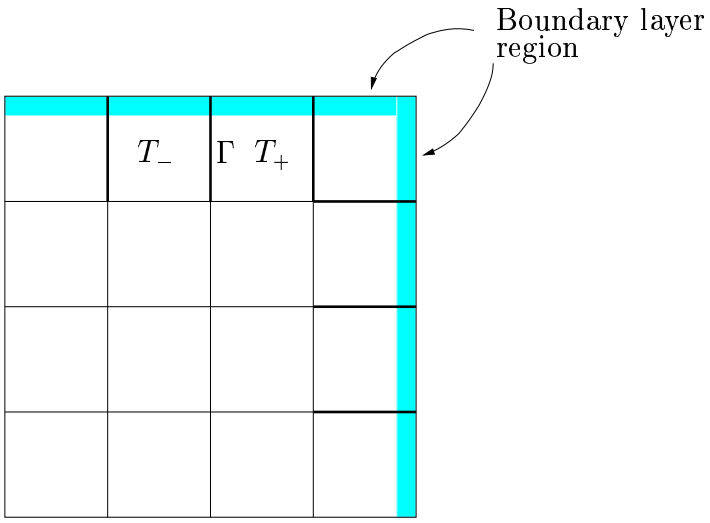

Figure 1: Axiparallel mesh. The edges where an edge-bubble is defined are marked.

where L_Γ is a differential operator obtained from L by considering directional derivatives along Γ. In our case, if for example Γ is parallel to the y-axis as in Figure 1, then L_Γ is obtained by discarding all terms with derivatives in the x-direction. More generally, when Γ is not aligned with a coordinate direction, since the Laplacian is rotation–invariant, we would define $L_\Gamma e_\Gamma = -\varepsilon e_\Gamma''(t) + a_\Gamma e_\Gamma'(t)$, where a_Γ is the projection of $\boldsymbol{a}$ along Γ.

Remark. To handle the case of convection–diffusion equations with symmetric tensor diffusion coefficient, we would need to freeze the diffusion coefficient to a constant tensor over the edge. Then a local rotation of the coordinate system and stretching along the rotated coordinate axis can be used to transform the diffusion term into the Laplacian.

This completely defines the space of edge-bubbles E_h and hence the RFBe method. We justify the choice of the edge-bubbles through a–priori analysis.

3.1 A-priori error analysis

We emphasise that the following analysis is valid under the hypothesis that $h \gtrsim \kappa$, where κ is the width of the boundary layer (see (3.5)). Of course, as the mesh is refined, the relative improvement in accuracy due to the introduction of edge-bubbles gradually diminishes (see the numerical examples below) and as h becomes smaller the standard RFB method will yield equally satisfactory results. Indeed, when $h \lesssim \kappa$, even a standard Galerkin finite element method will provide good accuracy. However, our concern here is the case when $h \gtrsim \kappa$.

To proceed, we shall strengthen our hypotheses on the mesh by assuming that it is

quasi-uniform, i.e. that there exists a constant $c_0 > 0$ such that

$$c_0 h \leq h_T \leq h = \max_{T \in \mathcal{T}} h_T, \tag{3.7}$$

for every $T \in \mathcal{T}$, where h_T is the diameter of the element T.

Before developing the a-priori analysis, we show that the global error of a locally residual-free finite element method is governed by the approximation properties of the augmented space V_a on the skeleton of the subdivision.

Let $u \in V$ and $u_a \in V_a$ be, respectively, the exact solution of (2.1) and its numerical approximation, the solution of (2.5). For any $v \in V_a$, using the appropriate coercivity inequality and Galerkin orthogonality, we have

$$\begin{aligned} \varepsilon |u - u_a|^2_{1,\Omega} &\leq \mathcal{L}(u - u_a, u - u_a) = \mathcal{L}(u - u_a, u - v) \\ &= \varepsilon \left(\nabla(u - u_a), \nabla(u - v)\right)_\Omega + (\boldsymbol{a} \cdot \nabla(u - u_a), u - v)_\Omega \\ &\leq C\varepsilon |u - u_a|_{1,\Omega} \left(|u - v|_{1,\Omega} + \varepsilon^{-1} ||u - v||_{0,\Omega}\right), \end{aligned}$$

where, as always in these pages, C represents a constant whose actual value may change value at different occurrences; C may be dependent on $\boldsymbol{a}$ but is always independent of ε and the mesh size h. Thus, for any $v \in V_a$,

$$\varepsilon |u - u_a|^2_{1,\Omega} \leq C \left(\varepsilon |u - v|^2_{1,\Omega} + \varepsilon^{-1} ||u - v||^2_{0,\Omega}\right). \tag{3.8}$$

To switch to norms defined over the skeleton of the triangulation, we use the following result from [16].

Lemma 3.1 *Assume that $\varepsilon < h \leq 1$, that (3.7) holds true and that the partition $\mathcal{T}$ is shape regular. Then, for each $T \in \mathcal{T}$, each $v_0 \in H^{1/2}(\partial T)$, and each $w \in H^1(T)$, there exists a function $v \in H^1(T)$ with $v = v_0$ on ∂T and satisfying*

$$\varepsilon \, |w - v|^2_{1,T} + \varepsilon^{-1} \, \|w - v\|^2_{0,T} \leq C \left(\varepsilon \, |w - v_0|^2_{1/2,\partial T} + \|w - v_0\|^2_{0,\partial T}\right), \tag{3.9}$$

where C depends only on $\mathcal{T}$.

We fix $v_0 \in V_P$ and consider its trace over the skeleton of the triangulation $\mathcal{T}$. Applying (3.9) with $w = u$ we have that, for some $v \in H^1_0(\Omega)$ which is equal to v_0 on the skeleton of $\mathcal{T}$,

$$\varepsilon \, |u - v|^2_{1,T} + \varepsilon^{-1} \, \|u - v\|^2_{0,T} \leq C \left(\varepsilon \, |u - v_0|^2_{1/2,\partial T} + \|u - v_0\|^2_{0,\partial T}\right),$$

for every $T \in \mathcal{T}$. Hence, since $v \in V_a$ and recalling (3.8), we conclude that

$$\varepsilon |u - u_a|^2_{1,\Omega} \leq C \inf_{v_0 \in V_P} \sum_{T \in \mathcal{T}} \left(\varepsilon \, |u - v_0|^2_{1/2,\partial T} + \|u - v_0\|^2_{0,\partial T}\right). \tag{3.10}$$

This inequality justifies the idea that the error can be reduced by enriching the trial space on the edges and represents the starting point for the a-priori error analysis of RFBe.

Theorem 3.2 *Let $u \in H_0^1(\Omega)$ be the solution of the boundary-value problem (3.1) assuming that $\varepsilon \in \mathbb{R}^+$, $f \in W_\infty^2(\Omega)$ and $\boldsymbol{a} = (a_1, a_2) \in [\mathcal{C}^1(\overline{\Omega})]^2$, with $\operatorname{div} \boldsymbol{a} \leq 0$ and $a_1, a_2 \geq c_a > 0$. Moreover, let $\mathcal{T}$ be an axiparallel rectangular mesh satisfying (3.7). Then, as long as $h \geq (1/2c_0c_a)\,\kappa$ and $\varepsilon \leq 1/\mathrm{e}$, the RFB solution $u_{RFB} \in V_{RFB} = V_h \oplus B_h$ satisfies*

$$\varepsilon^{1/2}|u - u_{RFB}|_{1,\Omega} + h^{-1/2}||\boldsymbol{a} \cdot \nabla(u - u_{RFB})||_{-1,\Omega} \leq C_1 \left(\varepsilon^{1/2}h^{-1/2} + \min\left(\varepsilon^{1/4}, h^{1/2}\right)\right) + C_2. \tag{3.11}$$

Let $u_a \in V_a = V_h \oplus E_h \oplus B_h$ be the RFBe solution where the edge bubbles are defined according to (2.10) and (3.19). Then, under the same hypotheses as above,

$$\varepsilon^{1/2}|u - u_a|_{1,\Omega} + h^{-1/2}||\boldsymbol{a} \cdot \nabla(u - u_a)||_{-1,\Omega} \leq C_1 \left(\varepsilon^{1/2}h^{-1/2} + \min\left(\varepsilon^{1/4}, h^{1/2}\right)\right) + C_3 h. \tag{3.12}$$

The constants C_1, C_2 and C_3 are independent of the mesh size h and of ε, but may depend on $\boldsymbol{a}$.

Remark. The error bounds stated in the theorem are still valid as long as the number of edges crossed by the characteristic curve through $(0,0)$ is of order $O(1/h)$, which is true under the hypothesis that $a_1, a_2 > 0$. In the absence of this assumption and requiring that $f \in W_\infty^1(\Omega)$ we obtain, by virtue of (3.17),

$$\varepsilon^{1/2}|u - u_a|_{1,\Omega} + h^{-1/2}||\boldsymbol{a} \cdot \nabla(u - u_a)||_{-1,\Omega} \leq C_1 \left(\varepsilon^{1/2}h^{-1/2} + h^{1/2}\right) + \begin{cases} C_2, & \text{for RFB} \\ C_3 h, & \text{for RFBe.} \end{cases}$$

Let us recall some trace inequalities which will be applied in the proof of the theorem. For any $v \in H^1(T)$, a scaling argument applied to the trace inequality $|v|^2_{1/2,\partial\widehat{T}} \leq C(||v||^2_{0,\widehat{T}} + |v|^2_{1,\widehat{T}})$, yields

$$|v|^2_{1/2,\partial T} \leq C\left(\frac{1}{h_T^2}||v||^2_{0,T} + |v|^2_{1,T}\right), \tag{3.13}$$

and a scaling argument applied to $|v|^2_{0,\partial\widehat{T}} \leq C(||v||^2_{0,\widehat{T}} + ||v||_{0,\widehat{T}}|v|_{1,\widehat{T}})$, yields

$$\begin{aligned} ||v||^2_{0,\partial T} &\leq C\left(h_T^{-1}||v||^2_{0,T} + |v|_{1,T}||v||_{0,T}\right) \\ &\leq C\left(h_T^{-1}||v||^2_{0,T} + \alpha^{-1}||v||^2_{0,T} + \alpha|v|^2_{1,T}\right), \end{aligned} \tag{3.14}$$

for any $\alpha > 0$ with C independent of v and α. Also by using a scaling argument we get

$$|v|_{1/2,\Gamma} \leq C\left(h_\Gamma^{-1}||v||_{0,\Gamma} + |v|_{1,\Gamma}||v||_{0,\Gamma}\right), \tag{3.15}$$

for any edge Γ of T, and any $v|_\Gamma \in H^1(\Gamma)$, where C is independent of v.

Proof. Applying (3.10) with $v_0 = u_{\rm as}^I$, an approximation of $u_{\rm as}$ from V_P which will be specified later, we have

$$\begin{aligned}
\varepsilon||u-u_a||^2_{1,\Omega} &\leq C\sum_{T\in\mathcal{T}}\left(\varepsilon|u-u_{\rm as}^I|^2_{1/2,\partial T}+||u-u_{\rm as}^I||^2_{0,\partial T}\right)\\
&\leq C\left(\sum_{T\in\mathcal{T}}\left(\varepsilon|u-u_{\rm as}|^2_{1/2,\partial T}+||u-u_{\rm as}||^2_{0,\partial T}\right)\right.\\
&\qquad\left.+\sum_{T\in\mathcal{T}}\left(\varepsilon|u_{\rm as}-u_{\rm as}^I|^2_{1/2,\partial T}+||u_{\rm as}-u_{\rm as}^I||^2_{0,\partial T}\right)\right)\\
&= C(I+II).
\end{aligned}$$

From our assumptions on ε and h it follows that $h \geq c\varepsilon$ with $c = 1/2c_0c_a$. Thus, using the trace inequalities (3.13) and (3.14) with $\alpha = \min\left(\varepsilon^{1/2}, h\right)$, and the bound for the asymptotic approximation (3.4), we get

$$\begin{aligned}
I &\leq C\sum_{T\in\mathcal{T}}\left((h_T^{-1}+\alpha^{-1})||u-u_{\rm as}||^2_{0,T}+(\varepsilon+\alpha)|u-u_{\rm as}|^2_{1,T}\right)\\
&\leq C\left((h^{-1}+\alpha^{-1})||u-u_{\rm as}||^2_{0,\Omega}+(\varepsilon+\alpha)|u-u_{\rm as}|^2_{1,\Omega}\right)\\
&\leq C\left(\varepsilon h^{-1}+\varepsilon\alpha^{-1}+\alpha\right)\\
&\leq C\left(\varepsilon h^{-1}+\min\left(\varepsilon^{1/2},h\right)\right).
\end{aligned}$$

Concerning II, we separate the contributions from those edges that cross the boundary layer (in which the edge bubbles are defined), and those that do not:

$$\begin{aligned}
II &\leq 2\sum_{\Gamma\in\Gamma_{\rm out}}\left(\varepsilon|u_{\rm as}-u_{\rm as}^I|^2_{1/2,\Gamma}+||u_{\rm as}-u_{\rm as}^I||^2_{0,\Gamma}\right)\\
&+ 2\sum_{\Gamma\in\Gamma_{\rm bl}}\left(\varepsilon|u_{\rm as}-u_{\rm as}^I|^2_{1/2,\Gamma}+||u_{\rm as}-u_{\rm as}^I||^2_{0,\Gamma}\right)\\
&= III+IV,
\end{aligned}$$

the factor 2 being due to the fact that we are now summing over edges Γ rather than through elements T as in the original definition of II.

Consider the decomposition $u_{\rm as} = u_0 + u_c$, where u_c represents the collection of all correction terms in (3.3). In the outside region, since $V_P = V_h$ and u_c is exponentially small, it is, therefore, natural to choose, on each edge Γ, $u_{\rm as}^I$ as the interpolant of $u_0|_\Gamma$.

Here we observe that, for every edge Γ, $u_0|_\Gamma \in H^1(\Gamma)$; moreover,

$$|u_0|^2_{1,\Gamma} \leq Ch_\Gamma. \tag{3.16}$$

Indeed, under our assumptions, $u_0 \in W^1_\infty(\Omega)$ and first order partial derivatives of u_0 can only have jump discontinuities across the characteristic courve passing through the corner of the inflow boundary (see, e.g. [15]). In the worst case scenario in which

such a characteristic curve divides Γ into two disjoint open intervals Γ_1 and Γ_2, since $u_{0|_{\Gamma_i}} \in W^1_\infty(\Gamma_i)$, $i = 1, 2$, we still have (assuming that Γ is parallel with the x–axis):

$$\begin{aligned} |u_0|^2_{1,\Gamma} &= |u_0|^2_{1,\Gamma_1} + |u_0|^2_{1,\Gamma_2} \\ &\leq \mathrm{meas}(\Gamma_1)\|u_{0,x}\|^2_{\mathrm{L}^\infty(\Gamma_1)} + \mathrm{meas}(\Gamma_2)\|u_{0,x}\|^2_{\mathrm{L}^\infty(\Gamma_2)} \\ &\leq \max\{\|u_{0,x}\|^2_{\mathrm{L}^\infty(\Gamma_1)}\,,\ \|u_{0,x}\|^2_{\mathrm{L}^\infty(\Gamma_2)}\}h_\Gamma \\ &= Ch_\Gamma. \end{aligned}$$

An identical bound holds when Γ is parallel with the y–axis.

Using the triangle inequality, (3.15) and a classical function space interpolation result we have

$$\begin{aligned} \varepsilon \sum_{\Gamma\in\Gamma_{\mathrm{out}}} |u_{\mathrm{as}} - u^I_{\mathrm{as}}|^2_{1/2,\Gamma} &\leq 2\varepsilon \sum_{\Gamma\in\Gamma_{\mathrm{out}}} \left(|u_0 - u^I_{\mathrm{as}}|^2_{1/2,\Gamma} + |u_c|^2_{1/2,\Gamma}\right) \\ &\leq C\varepsilon \left(\sum_{\Gamma\in\Gamma_{\mathrm{out}}} h_\Gamma |u_0|^2_{1,\Gamma} + \sum_{\Gamma\in\Gamma_{\mathrm{out}}} \left(h_\Gamma^{-1}||u_c||^2_{0,\Gamma} + |u_c|_{1,\Gamma}||u_c||_{0,\Gamma}\right) \right) \\ &\leq C\varepsilon \left(\sum_{\Gamma\in\Gamma_{\mathrm{out}}} h^2_\Gamma + \varepsilon \sum_{\Gamma\in\Gamma_{\mathrm{out}}} |u_c|^2_{1,\Gamma} + \varepsilon^{-1} \sum_{\Gamma\in\Gamma_{\mathrm{out}}} ||u_c||^2_{0,\Gamma} \right) \\ &\leq C\left(\varepsilon + \mathrm{e}^{-2c_0c_a h/\varepsilon}\right) \leq C\varepsilon, \end{aligned}$$

due to the estimates of the norms of u_c over the skeleton of the mesh given in Appendix A, and assuming, to obtain the last bound, that $h \geq (1/2c_0c_a)\,\varepsilon \ln(1/\varepsilon)$.

For the L_2–norm term in III, proceeding in the same fashion, we obtain

$$\begin{aligned} \sum_{\Gamma\in\Gamma_{\mathrm{out}}} ||u_{\mathrm{as}} - u^I_{\mathrm{as}}||^2_{0,\Gamma} &\leq \sum_{\Gamma\in\Gamma_{\mathrm{out}}} \left(||u_0 - u^I_{\mathrm{as}}||^2_{0,\Gamma} + ||u_c||^2_{0,\Gamma}\right) \\ &\leq C \left(\sum_{\Gamma\in\Gamma_{\mathrm{out}}} h^2_\Gamma |u_0|^2_{1,\Gamma} + \mathrm{e}^{-2c_0c_a h/\varepsilon} \right) \\ &\leq C \left(\sum_{\Gamma\in\Gamma_{\mathrm{out}}} h^3_\Gamma + \mathrm{e}^{-2c_0c_a h/\varepsilon} \right) \leq C\left(h + \mathrm{e}^{-2c_0c_a h/\varepsilon}\right) \leq Ch. \end{aligned}$$

After comparing the two bounds we conclude that

$$III \leq Ch. \tag{3.17}$$

Notice that we can obtain sharper bounds by carefully distinguishing between edges where u_0 has different regularity properties (as we already mentioned, u_0 may only fail to be a C^1 function across the characteristic curve that passes through the corner $(0, 0)$ on the inflow boundary). Suppose that $f \in W^2_\infty(\Omega)$. Let Γ_{ns} be the set of those edges that are crossed by the characteristic through $(0, 0)$; clearly, $\#(\Gamma_{\mathrm{ns}}) = O(1/h)$, due to

our hypothesis that $a_1, a_2 > 0$. Finally, let $\Gamma_{\rm sm} = \Gamma_{\rm out} \setminus \Gamma_{\rm ns}$ be the set of all edges where u_0 is smooth, i.e. $u_0|_\Gamma \in W^2_\infty(\Gamma)$, $\Gamma \in \Gamma_{\rm sm}$, and $u_0|_\Gamma \in W^1_\infty(\Gamma)$, $\Gamma \in \Gamma_{\rm ns}$. Then, we get

$$\begin{aligned}
\varepsilon \sum_{\Gamma\in\Gamma_{\rm out}} |u_0 - u^I_{\rm as}|^2_{1/2,\Gamma} &= \varepsilon \left(\sum_{\Gamma\in\Gamma_{\rm sm}} |u_0 - u^I_{\rm as}|^2_{1/2,\Gamma} + \sum_{\Gamma\in\Gamma_{\rm ns}} |u_0 - u^I_{\rm as}|^2_{1/2,\Gamma} \right) \\
&\le C\varepsilon \left(\sum_{\Gamma\in\Gamma_{\rm sm}} h^3_\Gamma |u_0|^2_{2,\Gamma} + \sum_{\Gamma\in\Gamma_{\rm ns}} h_\Gamma |u_0|^2_{1,\Gamma} \right) \\
&\le C\varepsilon \left(\sum_{\Gamma\in\Gamma_{\rm sm}} h^4_\Gamma + \sum_{\Gamma\in\Gamma_{\rm ns}} h^2_\Gamma \right) \\
&\le C\varepsilon(h^2 + h) \le C\varepsilon h.
\end{aligned}$$

Similarly, we gain a factor of h in the bound for the L_2–norm, and we conclude that

$$III \le Ch^2.$$

We now come to the analysis of IV, i.e. the term containing norms of $u_{\rm as} - u^I_{\rm as}$ over those edges that intersect the boundary layer.

If $V_P = V_h$, that is for the RFB method, since the first derivative of $u_{\rm as}$ is very large within boundary layers, it is not advisable to make use of the standard bounds on the error in linear interpolation to estimate $u_{\rm as} - u^I_{\rm as}$. Instead, we shall simply apply the triangle inequality and bound each term individually.

Let us concentrate on the boundary layer associated with the boundary $y = 1$. For any edge $\Gamma_i = x_i \times [1 - h_\Gamma, 1]$, $i = 1, \ldots, m-1$, since we have already fixed $u^I_{\rm as}(x_i, 1 - h_\Gamma) = u_0(x_i, 1 - h_\Gamma)$, we have

$$u^I_{{\rm as}|_{\Gamma_i}} = u_0(x_i, 1 - h_\Gamma)\frac{1 - y}{h_\Gamma}.$$

By recalling the definition of the seminorm $|\cdot|_{1/2,\Gamma_i}$, we easily see that

$$|u^I_{\rm as}|^2_{1/2,\Gamma_i} \le C.$$

Of course, an analogous result holds on the edges adjacent to the boundary $x = 1$. Thus, writing as before $u_{\rm as} - u^I_{\rm as} = u_0 - u^I_{\rm as} + u_c$, applying (3.15) and noting that $\#(\Gamma_{\rm bl}) = O(1/h)$, we obtain:

$$\begin{aligned}
\varepsilon \sum_{\Gamma\in\Gamma_{\rm bl}} |u_{\rm as} - u^I_{\rm as}|^2_{1/2,\Gamma} &\le 3\varepsilon \sum_{\Gamma\in\Gamma_{\rm bl}} \left(|u_0|^2_{1/2,\Gamma} + |u^I_{\rm as}|^2_{1/2,\Gamma} + |u_c|^2_{1/2,\Gamma} \right) \\
&\le 3\varepsilon \sum_{\Gamma\in\Gamma_{\rm bl}} \left(Ch_\Gamma + C + h^{-1}_\Gamma ||u_c||^2_{0,\Gamma} + |u_c|_{1,\Gamma}||u_c||_{0,\Gamma} \right) \\
&\le C \left(\varepsilon h^{-1} + \varepsilon^2 \sum_{\Gamma\in\Gamma_{\rm bl}} |u_c|^2_{1,\Gamma} + \sum_{\Gamma\in\Gamma_{\rm bl}} ||u_c||^2_{0,\Gamma} \right) \\
&\le C\varepsilon h^{-1},
\end{aligned}$$

thanks again to a bound given in Appendix A. Similarly, for the L_2–norm term we obtain

$$\begin{aligned}\sum_{\Gamma\in\Gamma_{\rm bl}} ||u_{\rm as}-u_{\rm as}^I||_{0,\Gamma}^2 &\le 3\sum_{\Gamma\in\Gamma_{\rm bl}}\left(||u_0||_{0,\Gamma}^2+||u_{\rm as}^I||_{0,\Gamma}^2+||u_c||_{0,\Gamma}^2\right)\\ &\le C\sum_{\Gamma\in\Gamma_{\rm bl}} h_\Gamma+\sum_{\Gamma\in\Gamma_{\rm bl}}||u_c||_{0,\Gamma}^2\\ &\le C\left(1+\varepsilon h^{-1}\right)\le C.\end{aligned}$$

Thus, for the RFB method,

$$IV\le C. \tag{3.18}$$

By considering the case $V_P=V_h\oplus E_h$, we now show that the edge-bubbles proposed above provide the required extra resolution in the boundary layer.

This time, for any edge $\Gamma_i=x_i\times[1-h_\Gamma,1]$, $i=1,\ldots,m-1$, we still have one degree of freedom (the edge bubble) at our disposal. That is,

$$u_{{\rm as}|_{\Gamma_i}}^I=u_0(x_i,1-h_\Gamma)\frac{1-y}{h_\Gamma}+\gamma_i e_{\Gamma_i},$$

for some coefficient $\gamma_i\in\mathbb{R}$ which we are free to choose.

We consider the following decomposition of the asymptotic approximation $u_{\rm as}(x,y)$ of $u(x,y)$:

$$\begin{aligned}u_{\rm as}(x_i,y) &= u_0(x_i,y)-u_0(x_i,1)\mathrm{e}^{-a_2(x_i,1)\frac{1-y}{\varepsilon}}\\ &+ \left(-u_0(1,y)\mathrm{e}^{-a_1(1,y)\frac{1-x_i}{\varepsilon}}+u_0(1,1)\mathrm{e}^{-a_1(1,1)\frac{1-x_i}{\varepsilon}}\mathrm{e}^{-a_2(1,1)\frac{1-y}{\varepsilon}}\right)\\ &=: u_0^i(y)+u_{c_y}^i(y)+u_c^i(y).\end{aligned}$$

The function u_c^i collects the correction terms related to the boundary layer at $x=1$ and to the corner layer, which are, as before, exponentially small. Hence, the main task is to define $u_{{\rm as}|_\Gamma}^I$ as a good approximation of $u_0^i+u_{c_y}^i$.

Let $l(u_{c_y}^i)$ be the linear function that interpolates $u_{c_y}^i$ on Γ_i, and consider the decomposition

$$u_0^i+u_{c_y}^i=\left(u_0+l(u_{c_y}^i)\right)+\left(u_{c_y}^i-l(u_{c_y}^i)\right).$$

We observe that $u_{c_y}^i-l(u_{c_y}^i)$ conforms with our definition of edge bubble since it solves the homogeneous boundary-value problem

$$\begin{cases} L_{\Gamma_i}w=a_2(x_i,1)\frac{u_{c_y}^i(1-h_\Gamma)-u_{c_y}^i(1)}{h_\Gamma} & \text{on }\Gamma_i\,,\\ w_{|\partial\Gamma_i}=0,\end{cases}$$

where

$$L_{\Gamma_i}w:=-\varepsilon w''+a_2(x_i,1)w'. \tag{3.19}$$

Thus, with such a definition of L_{Γ_i} and recalling (3.6), we obtain $\gamma_i e_{\Gamma_i} = u^i_{c_y} - l(u^i_{c_y})$ by setting

$$\gamma_i := a_2(x_i,1)\frac{u^i_{c_y}(1-h_{\Gamma_i}) - u^i_{c_y}(1)}{h_\Gamma}.$$

In this way, recalling the definition of $u^I_{\rm as}|_{\Gamma_i}$,

$$\begin{aligned}
u^i_0 + u^i_{c_y} - u^I_{{\rm as}|_{\Gamma_i}} &= \Big(u^i_0 + l(u^i_{c_y})\Big) + \Big(u^i_{c_y} - l(u^i_{c_y})\Big) - \left(u^i_0(1-h_\Gamma)\frac{1-y}{h_\Gamma} + \gamma_i e_{\Gamma_i}\right) \\
&= u^i_0 + l(u^i_{c_y}) - u^i_0(1-h_\Gamma)\frac{1-y}{h_\Gamma} \\
&= u^i_0 + u^i_{c_y}(1)\frac{y-1+h_\Gamma}{h_\Gamma} + u^i_{c_y}(1-h_\Gamma)\frac{1-y}{h_\Gamma} - u^i_0(1-h_\Gamma)\frac{1-y}{h_\Gamma} \\
&= u^i_0 - l(u^i_0) + u^i_{c_y}(1-h_\Gamma)\frac{1-y}{h_\Gamma},
\end{aligned}$$

since $u^i_{c_y}(1) = -u^i_0(1)$. As before, the notation $l(\cdot)$ stands for linear interpolation.

We are now ready to bound IV. By the triangle inequality, a classical function space interpolation result and (3.16),

$$\begin{aligned}
&\varepsilon \sum_{i=1}^{m-1} |u_{\rm as}(x_i,\cdot) - u^I_{\rm as}(x_i,\cdot)|^2_{1/2,\Gamma_i} \\
&\qquad \le 2\,\varepsilon \sum_{i=1}^{m-1} \Big(|u^i_0 + u^i_{c_y} - u^I_{\rm as}|^2_{1/2,\Gamma_i} + |u^i_c|^2_{1/2,\Gamma_i}\Big) \\
&\qquad = 2\,\varepsilon \sum_{i=1}^{m-1} \left(\left|u^i_0 - l(u^i_0) + u^i_{c_y}(1-h_\Gamma)\frac{1-y}{h_\Gamma}\right|^2_{1/2,\Gamma_i} + |u^i_c|^2_{1/2,\Gamma_i}\right) \\
&\qquad \le 2\,\varepsilon \sum_{i=1}^{m-1} \Big(2|u^i_0 - l(u^i_0)|^2_{1/2,\Gamma_i} + 2C|u^i_{c_y}(1-h_\Gamma)|^2 + |u^i_c|^2_{1/2,\Gamma_i}\Big) \\
&\qquad \le C\varepsilon \sum_{i=1}^{m-1} \big(h_\Gamma |u^i_0|^2_{1,\Gamma_i} + {\rm e}^{-2a_2(x_i,1)h_\Gamma/\varepsilon} + |u^i_c|^2_{1/2,\Gamma_i}\big) \\
&\qquad \le C(\varepsilon h + \varepsilon^2 h^{-1}) \le C\varepsilon h,
\end{aligned}$$

since $|u^i_c|^2_{1/2,\Gamma_i}$ is exponentially small and $h \ge c\varepsilon$. Similarly,

$$\begin{aligned}
\sum_{i=1}^{m-1} ||u_{\rm as}(x_i,\cdot) - u^I_{\rm as}(x_i,\cdot)||^2_{0,\Gamma_i} &\le C\sum_{i=1}^{m-1} \big(h^2_\Gamma |u^i_0|^2_{1,\Gamma_i} + h_\Gamma {\rm e}^{-2a_2(x_i,1)h_\Gamma/\varepsilon} + ||u^i_c||^2_{0,\Gamma_i}\big) \\
&\le C(h^2+\varepsilon).
\end{aligned}$$

Thus we have shown that

$$IV \le C(h^2+\varepsilon).$$

Finally, recalling from [17] that the streamline derivative of the error

$$||\boldsymbol{a}\cdot\nabla(u-u_a)||_{-1,\Omega} := \sup_{v\in H^1(\Omega)} \frac{\int_\Omega \boldsymbol{a}\cdot\nabla(u-u_a)v\,d\Omega}{|v|_{1,\Omega}}$$

is controlled by the energy norm error, in the sense that

$$h^{-1/2}||\boldsymbol{a}\cdot\nabla(u-u_a)||_{-1,\Omega} \le C\varepsilon^{1/2}|u-u_a|_{1,\Omega},$$

we deduce that (3.11) and (3.12) hold. □

We conclude this section with some comments. The correct choice of the edge–bubbles on the edges is hinted by the error analysis. In particular, the edge-bubble is chosen to be equal to the boundary layer correction term in the asymptotic approximation of the solution while bounding the interpolation error $u_{\rm as}-u_{\rm as}^I$. This choice resulted in the $O(h)$ term in the error bound (3.12).

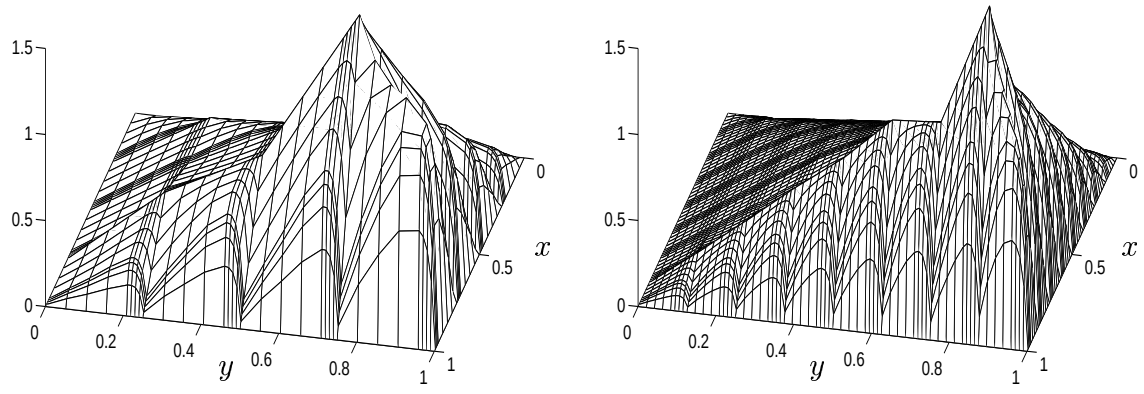

(a) $h = 1/4$ (b) $h = 1/8$

Figure 2: The RFB solution of the problem of Example 2. The problem parameters are $\varepsilon = 10^{-2}$, $\boldsymbol{a} = (\cos(\pi/4), \sin(\pi/4))$.

In the context of convection-diffusion problems, we say that a method is uniformly convergent of order α with respect to some norm $||\cdot||_\varepsilon$ (which may depend on ε), if an error bound of the form

$$||u-u_h||_\varepsilon \le Ch^\alpha,$$

holds for some positive constant α that is independent of ε as $h \to 0$. In the preasymptotic regime, when $\varepsilon \ll h$, we observe for the RFBe method that $\sqrt{\varepsilon}|u - u_a|_{1,\Omega} \leq Ch$, with C independent of ε.

It is interesting to note that all methods studied in the literature that achieve uniform convergence on shape-regular partitions are based on the use of ad-hoc exponential basis functions (see [15], pp. 273-8). In particular, we refer to the conforming methods in [14] and [19] and the non-conforming method in [1]. All such methods consider exponentially fitted splines as trial and test spaces, constructed as tensor products of solutions of the restriction of the original equation on the edges. They all achieve uniform rate of convergence with $\alpha = 1/2$ in the $\sqrt{\varepsilon}$-weighted energy norm.

The method by Schieweck [19], similarly to our method, considers basis functions constructed using exponentials only on those edges which cross the boundary layer. Elsewhere, it uses a standard bilinear approximation. Schieweck proves that, for his method,

$$\varepsilon^{1/2}|u - u_h|_{1,\Omega} \leq C\left((\varepsilon/h)^{1/2} + h^{1/2}\right).$$

Our method can be seen as a combination of the residual–free bubble method with exponential fitting on edges contained in the boundary layer.

We know from the local a-priori error analysis of Sangalli [16] that, for $\varepsilon \ll h$, away from the boundary layer region, the RFB method is also $O(h)$ accurate in the energy norm. Our error bounds show that an identical result cannot hold in the energy norm on the whole Ω, unless the approximation properties in the layers are improved. Moreover, we have identified the inferior approximation of the boundary layer behavior along the edges of the triangulation as the main source of the inaccuracy of the RFB method. This observation will also be confirmed by our numerical experiments.

Figure 2 may help to clarify why refining the mesh need not improve the accuracy of the RFB method in the preasymptotic regime of $h \gtrsim \varepsilon$. The plots show the RFB approximation to the solution of the boundary-value problem described in Example 2 below on two subsequent uniform meshes. The lengths of the edges crossing the boundary layer are halved as we half the mesh size, but the number of such edges is doubled. Hence convergence is impeded until the mesh starts to resolve the boundary layer.

This argument, of course, can also be seen as further evidence of the advantages of anisotropic mesh refinement. Indeed, returning to the bound (3.18) on term IV which does not imply convergence of term IV to zero under mesh refinement, we see that this is due to the fact that

$$\sum_{\Gamma \in \Gamma_{\rm bl}} h_\Gamma = h_\Gamma \, \#(\Gamma_{\rm bl}).$$

Hence, on a succession of anisotropically refined meshes, graded in the normal direction to the boundary layer, we achieve reduction of h_Γ (whilst keeping $\#(\Gamma_{\rm bl})$ fixed), and hence we should expect improvement in the accuracy of the solution.

4 Full discretisation and numerical examples

As discussed in Section 2, one can consider different splittings of V_{RFB}, the only constraint being that each element of V_{RFB} must be linear on every edge of the triangulation.

For each $v_h \in V_h$ we define $\widetilde{v}_h \in V_{RFB}$ such that

$$\begin{cases} \widetilde{v}_h - v_h \in B_h & \text{and} \\ \mathcal{L}(\widetilde{v}_h, v_b) = 0 & \forall v_b \in B_h. \end{cases} \tag{4.1}$$

In this way we construct a new subspace $\widetilde{V}_h$ which coincides with the space V_l as defined in (2.6). Moreover, we still have

$$V_{RFB} = \widetilde{V}_h \oplus B_h,$$

which again leads to the augmented space formulation discussed in Section 2. Similarly, $V_a = \widetilde{V}_h \oplus E_h \oplus B_h$ where, this time, $\widetilde{V}_h \oplus E_h = V_l$, and the unique solution of (2.12) can be rewritten as $u_a = \widetilde{u}_h + u_e + u_b^f$ where, as we have seen in Section 2, u_b^f is the solution of

$$\mathcal{L}(u_b^f, v_b) = (f, v_b) \qquad \forall v_b \in B_h.$$

Equivalently, $u_{b\,|_T}^f = b_f$ for any $T \in \mathcal{T}$, where b_f solves (2.16). Further, testing with $w_h \in \widetilde{V}_h \oplus E_h$, we have that $\widetilde{u}_h + u_e$ satisfies

$$\mathcal{L}(\widetilde{u}_h + u_e, w_h) = (f, w_h) - \sum_{T \in \mathcal{T}} \mathcal{L}(b_f, w_h) \qquad \forall w_h \in \widetilde{V}_h \oplus E_h, \tag{4.2}$$

which is equivalent to (2.9).

The formulation (4.2) is similar to the *multiscale finite element method* (MFEM) defined in [11] for the solution of symmetric elliptic problems, enhanced by edge–bubbles. The MFEM method is a Galerkin method in which the local basis functions are defined by solving boundary value problems for the original equation. In our case, given an element $T \in \mathcal{T}$ and letting $\{\varphi_i\}_{i=1}^4$ be the standard bilinear basis functions related to T, the corresponding basis functions $\{\widetilde{\varphi}_i\}_{i=1}^4$ for the space $\widetilde{V}_h$ are obtained, according to (4.1), by solving, for $i = 1, 2, 3, 4$, the local boundary-value problems

$$\begin{cases} \widetilde{\varphi}_i \in H^1(T) \text{ such that} \\ \mathcal{L}(\widetilde{\varphi}_i, v_b) = 0 \quad \forall v_b \in H_0^1(T) \\ \mathrm{Tr}(\widetilde{\varphi}_i) = \varphi_i \qquad \text{on } \partial T. \end{cases} \tag{4.3}$$

Since the basis functions have to be evaluated numerically, the algorithm is, clearly, of a two-level type.

We have chosen to use the formulation (4.2)-(4.3) as the starting point for the full discretisation of the method. Once more, we would like to stress the fact that the two formulations, (2.17) and (4.2), are equivalent. Moreover the two approaches involve the

same number of subgrid computations. Nevertheless, we have found that the formulation given by (4.2) is simpler to code and results in slightly faster computations.

In order to solve the boundary-value problems that define the basis functions of V_a, we need to introduce a subgrid. We do so by considering a sub-partition $\mathcal{T}_N$ of the original triangulation, where N is the discretization parameter of the new partition. The restriction of $\mathcal{T}_N$ to any element $T \in \mathcal{T}$ defines a triangulation of T that we use to solve the problems (4.3), (2.16) and (2.10) which define, respectively, the local basis for the space $\widetilde{V}_h$, the bubble related to the forcing term and, finally, the edge bubbles.

Accordingly, on selecting V^N as the bilinear finite element space over $\mathcal{T}_N$, we define:

1. the discrete counterpart of the bubble space (2.3) as

$$B^N = B_h \cap V^N;$$

2. the space of edge-bubbles as the subspace of V^N given by

$$E^N = \text{span}\,\{e_j^N,\, j = 1, \ldots, N_e\} \subset V^N,$$

   where e_j^N is obtained by solving in V^N the boundary value problem (2.10) ;

3. the discrete counterpart $\widetilde{V}_h^N$ of $\widetilde{V}_h$ as

$$\text{span}\,\{\widetilde{\varphi}_i^N,\, i = 1, \ldots, 4\} \qquad \forall T \in \mathcal{T},$$

   where $\widetilde{\varphi}_i^N = \widetilde{\varphi}_i^{N,T}$ is the solution in V^N of (4.3) on $T \in \mathcal{T}$.

The fully discrete RFBe space is then defined as

$$V_a^N = \widetilde{V}_h^N \oplus E^N \oplus B^N,$$

and the fully discrete RFBe formulation reads

$$\begin{cases} \text{find } u_a^N \in V_a^N \text{ such that} \\ \mathcal{L}(u_a^N, v_a^N) = (f, v_a^N) \qquad \forall v_a^N \in V_a^N, \end{cases} \tag{4.4}$$

and can be again rewritten in the form (4.2).

The analytical study of the size of the additional error due to the introduction of the subgrid (*subgrid discretisation error*) in the fully discrete formulation (4.4) does not appear to be straight forward; the main difficulty being that Lemma 3.1 is no longer applicable at the fully discrete level. Thus, we shall assess the impact of subgrid discretisation on the accuracy of the method through numerical experiments.

4.1 Numerical examples

We now present some numerical experiments, carried out in MATLAB, using the formulation (4.4) in order to validate the a-priori error analysis and assess the size of the numerical error due to the discretisation at the subgrid level.

Example 1. We consider the boundary–value problem

$$\begin{cases} Lu := -\varepsilon \Delta u + \boldsymbol{a} \cdot \nabla u = f & \text{in } \Omega, \\ u = g & \text{on } \partial\Omega, \end{cases}$$

where

$$\boldsymbol{a} = \frac{3 - xy}{2}(1,1); \qquad f = 2; \qquad g = \begin{cases} \frac{1}{2}(1 + \cos(5\pi x)) & \text{if } y = 0 \\ \frac{1}{2}(1 + \cos(3\pi y)) & \text{if } x = 0 \\ 0 & \text{otherwise;} \end{cases}$$

see Figure 3 for a sample solution corresponding to $\varepsilon = 1/50$.

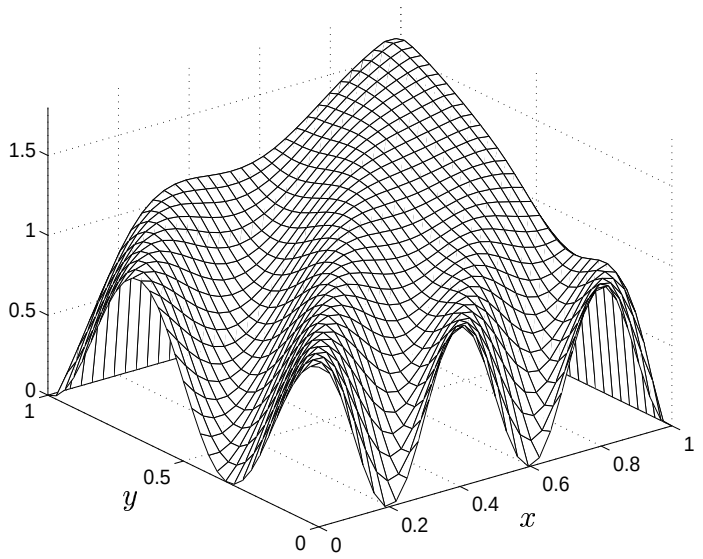

Figure 3: Example 1. Solution on a 32×32 uniform mesh, $\varepsilon = 1/50$.

We solve this model problem on a sequence of uniform meshes using both the RFB and the RFBe methods. For each computation, the subgrid mesh is axiparallel and of Shishkin type with turning point $\lambda = c_s \frac{\varepsilon}{c_a} \ln N$ and the same value of the Shishkin parameter $c_s = 1/4$; see Appendix B for more details regarding Shishkin meshes.

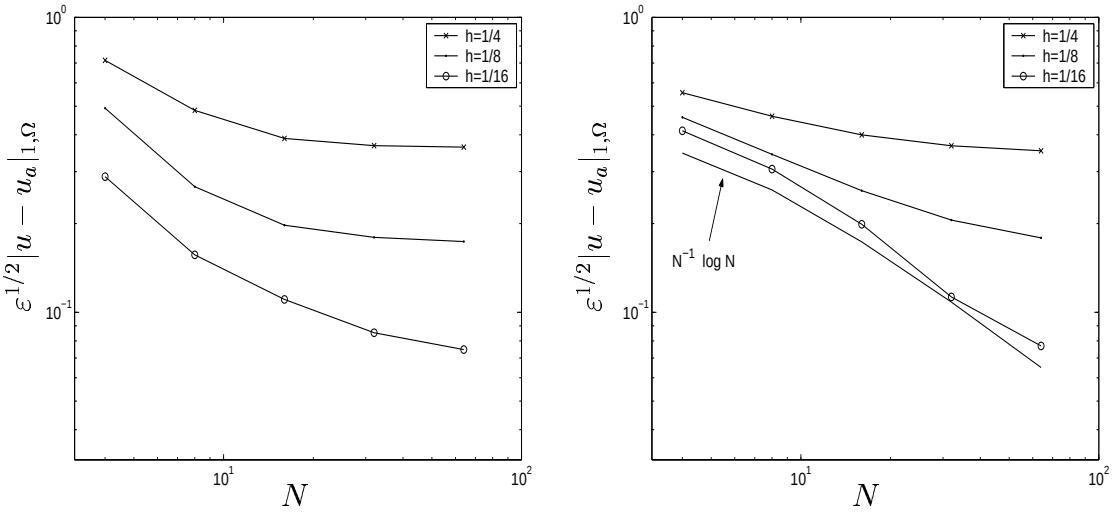

(a) Error vs. N, $\varepsilon = 1/50$

(b) Error vs. N, $\varepsilon = 10^{-2}$

Figure 4: Example 1. $\sqrt{\varepsilon}$-weighted energy norm error as a function of N.

We wish to confirm the a-priori bounds on the energy-norm error both in terms of the mesh size h and the diffusion parameter ε. In order to do so, we need to ensure that the subgrid computations are accurate enough.

Figures 4(a) and 4(b) show the global error in the $\sqrt{\varepsilon}$-weighted energy norm for a fixed mesh size but different values of the subgrid mesh parameter N for, respectively, $\varepsilon = 1/50$ and $\varepsilon = 10^{-2}$.

We notice that a substantial reduction of the error is obtained just by refining the subgrid, until the macro discretisation error becomes dominant and refining the subgrid thereon yields no improvement in the overall accuracy. This happens later for smaller values of ε and h. For instance, for $\varepsilon = 10^{-2}$ and $h = 1/16$ (see Figure 4(b)), we initially observe the characteristic $N^{-1} \log N$ convergence rate on Shishkin meshes (see Appendix B), showing that the subgrid discretisation error dominates the overall computational error in this case.

Based on such computational evidence, we may infer that the error bound for the fully discrete method should include a term proportional to the error in the numerical approximation of the elemental basis functions. This would be in accordance with the findings of Sangalli [17] on a different augmented RFB formulation applied to a symmetric problem. (For the problems considered in [17], Sangalli's argument is applicable to our method as well).

The convergence in terms of the mesh parameter h is shown in the log-log plots of Figure 5. Since we do not have at hand the exact solution, the error is evaluated using a reference solution given by Richardson extrapolation using two numerical solutions obtained on Shishkin–type meshes with, respectively, 256 and 512 nodes in each coordinate direction.

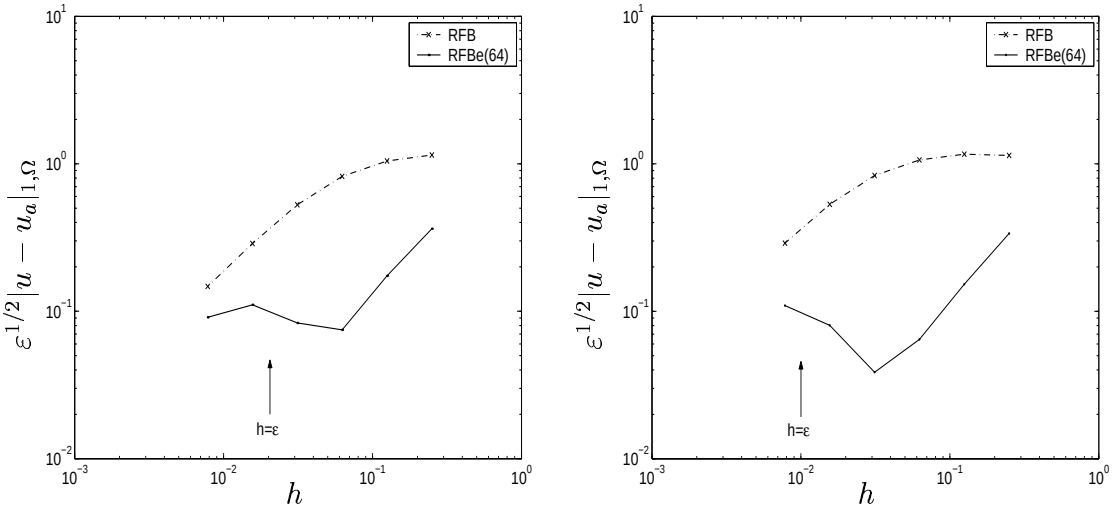

(a) Error vs. h, $\varepsilon = 1/50$

(b) Error vs. h, $\varepsilon = 10^{-2}$

Figure 5: Example 1. $\sqrt{\varepsilon}$-weighted energy norm error as a function of h: RFB method and RFBe method with $N = 64$ (RFBe(64)).

The RFBe solution initially converges to the reference solution with rate 1. As we keep refining, the slope of the error curve changes sign (the rate becomes approximately $-1/2$) until the error curve joins the corresponding error curve for the RFB method (the rates are listed in Table 1).

The relatively inaccurate results obtained when $h \sim \varepsilon$ are easy to explain. The region $\Omega_{\rm bl}$, i.e. the union of the elements enriched with the edge-bubbles, is properly contained in the boundary layer region, hence part of the boundary layer behaviour cannot be accurately captured. Eventually, the mesh is fine enough to resolve the layer, and the asymptotic convergence rate of the method is then recovered.

As for the subgrid computations, we have used the value $N = 64$ (hence the notation

	$\varepsilon = 1/50$				$\varepsilon = 10^{-2}$			
h	Energy	rate	L_2	rate	Energy	rate	L_2	rate
1/4	0.363		0.141		0.337		0.17	
1/8	0.174	1.06	0.043	1.7	0.152	1.14	0.051	1.73
1/16	0.074	1.22	0.011	1.92	0.064	1.24	0.0138	1.89
1/32	0.083	−0.15	0.0042	1.43	0.038	0.74	0.0036	1.93
1/64	0.11	−0.41	0.0025	0.77	0.08	−1.05	0.0025	0.53
1/128	0.091	0.28	0.00103	1.28	0.109	−0.45	0.0017	0.55

Table 1: Example 1. Error and convergence rate for RFBe(64).

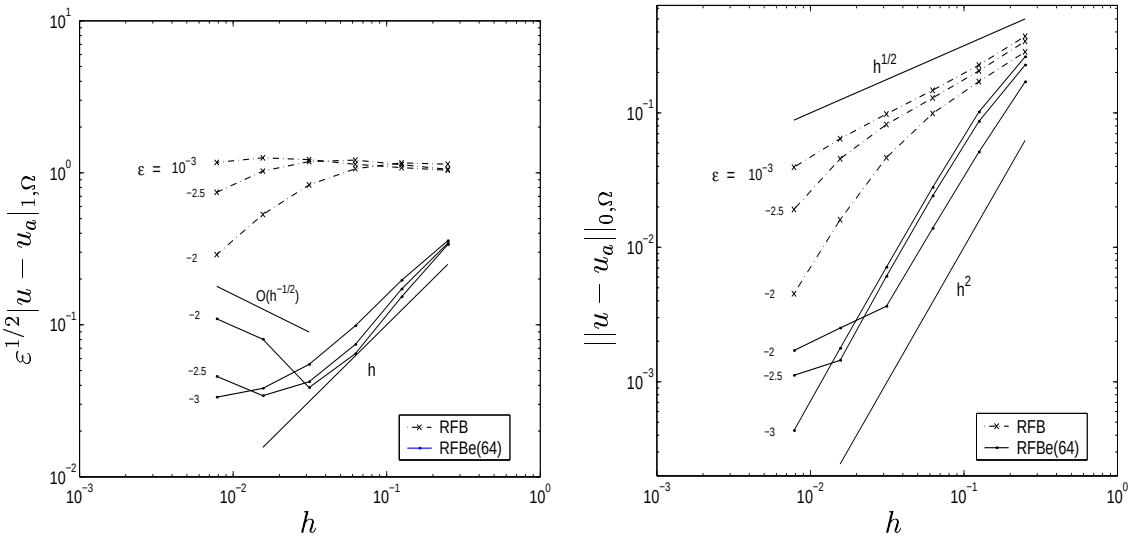

(a) $\sqrt{\varepsilon}$-weighted energy norm error

(b) L_2-norm error

Figure 6: Example 1. Error as a function of h for different values of ε: the RFB method and the RFBe method with subgrid discretisation parameter $N = 64$ (RFBe(64)).

RFBe(64)). As we see from Figure 4, this choice ensures that the subgrid discretisation error is of lower order. For smaller values of ε we can still identify the rate of convergence predicted by the a-priori analysis; see Figure 6(a).

As regards the L^2-norm error, not covered by our theorem, the RFBe method seems to be second-order 'convergent' in the preasymptotic regime when $\varepsilon \ll h$. The local a-priori analysis of Sangalli [16] predicts the same rate of convergence for RFB in the outside region.

So far we have not taken into account computational cost. The RFBe method is computationally more expensive then RFB on the same triangulation since it involves a larger number of degrees of freedom, and because the extra d.o.f., the edge bubbles, need to be computed.

Assume that the triangulation is uniform with $n \times n$ elements; the number of edge-bubbles is then $2(n-1)$, while the total number of d.o.f. is of $O(n^2)$. Moreover, assume that the basis functions (4.3) are calculated using a 4×4 subgrid, as in all computations presented so far. As for the edge bubbles, we are free to consider finer subgrids. We then have a range of possible scenarios. If, for example, also the edge-bubbles are computed on 4×4 subgrids, the computational time for the two methods (RFB and RFBe) is almost identical. On the other hand, if relatively fine subgrids are used for the edge-bubbles (32×32 in our example below), the CPU time is dominated by the computation of the edge-bubbles, hence RFBe becomes much more expensive.

Nevertheless, since the boundary layer is a major source of error, the RFBe method

	$\varepsilon = 10^{-2}$			
TOL	RFBe(32)	RFBe(4)	RFB	Galerkin
1/2	6 [3]	2.2 [10]	77 [68]	14 [94]
1/5	16 [7]	59 [58]		
1/10	46 [18]			

Table 2: Example 1. Computational time (in seconds) to achieve, on a uniform mesh, a given accuracy (TOL) in the $\sqrt{\varepsilon}$-weighted H^1-norm. We indicate in square brackets the number of elements used in each coordinate direction on the global uniform mesh. RFBe(N) indicates that an $N \times N$ subgrid was used for computing the edge bubbles. A 4×4 subgrid is used to compute the RFB (internal) bubbles in each case.

can be more effective even if the edge-bubbles are calculated with high precision. This is particularly true if we require a certain accuracy in the energy norm of the solution. In the Table 2, we compare the computational time necessary for the RFBe(32), RFBe(4), RFB methods and that of a standard Galerkin finite element method to compute the solution to a fixed tolerance (TOL) in the $\sqrt{\varepsilon}$-weighted energy norm, for $\varepsilon = 10^{-2}$. The table reports the CPU time in seconds on a Pentium III 800 MHz processor; the corresponding number of elements on each coordinate direction is given by the numbers in square brackets. We have left the entries of the table blank if to achieve the required accuracy a *resolving* mesh was necessary, i.e. if $n > 100$.

We notice that the RFB and Galerkin methods are unable to provide any reasonable accuracy in the energy norm on unresolving meshes. This situation would become even more evident if we were to consider problems with smaller values of ε. Having said this, the accuracy of the RFBe method on unresolving meshes is also limited albeit to a much lesser extent than the accuracy of RFB and standard Galerkin methods (cf. Figure 6).

Similarly, Table 3 reports the computational time to achieve a fixed accuracy in the L^2-norm, for $\varepsilon = 10^{-2}$, 10^{-3} and 10^{-4}.

Again, the RFBe method is the most effective in almost all the cases considered, in particular for the lower values of ε. More precisely, we notice the following:

1. For RFBe(32), the evaluation of the edge-bubbles takes almost all the CPU time.

2. While this is the case, the growth of the computational time is roughly linear, while the method is converging quadratically (again, see Figure 6).

3. On the other hand, the computational cost of all the other methods considered grows quadratically, while their rate of convergence is less then quadratic.

Hence, as the tolerance becomes tighter, the RFBe(32) method requires a smaller amount of CPU time than the other methods.

Finally, we remark that the mesh used to evaluate the basis functions (the internal bubbles if we think in terms of RFB) could also be adjusted. The presence of the edge bubbles improves the stability of the RFB method (as we shall show in the next

	$\varepsilon = 10^{-4}$			
TOL	RFBe(32)	RFBe(4)	RFB	Galerkin
1/5	14 [5]	1 [6]	1.1 [8]	272 [200]
1/10	26 [9]	2.2 [10]	14 [30]	
1/50	52 [20]	105 [78]		
1/100	92 [28]			

	$\varepsilon = 10^{-3}$			
TOL	RFBe(32)	RFBe(4)	RFB	Galerkin
1/5	14 [5]	1 [6]	1.8 [10]	5 [62]
1/10	22 [8]	2 [9]	17 [32]	32 [120]
1/50	49 [19]	39 [46]		
1/100	71 [26]	124 [84]		

	$\varepsilon = 10^{-2}$			
TOL	RFBe(32)	RFBe(4)	RFB	Gal
1/5	6 [3]	0.6 [4]	1 [6]	0.3 [17]
1/10	14 [6]	1 [6]	2 [16]	0.8 [28]
1/50	35 [14]	4.5 [15]	52 [56]	7 [74]
1/100	52 [20]	9 [22]	137 [90]	21 [106]

Table 3: Example 1. Computational time (in seconds) to achieve, on a uniform mesh, a given accuracy (TOL) in the L^2-norm. We indicate in square brackets, the number of elements used in each coordinate direction on the global uniform mesh.

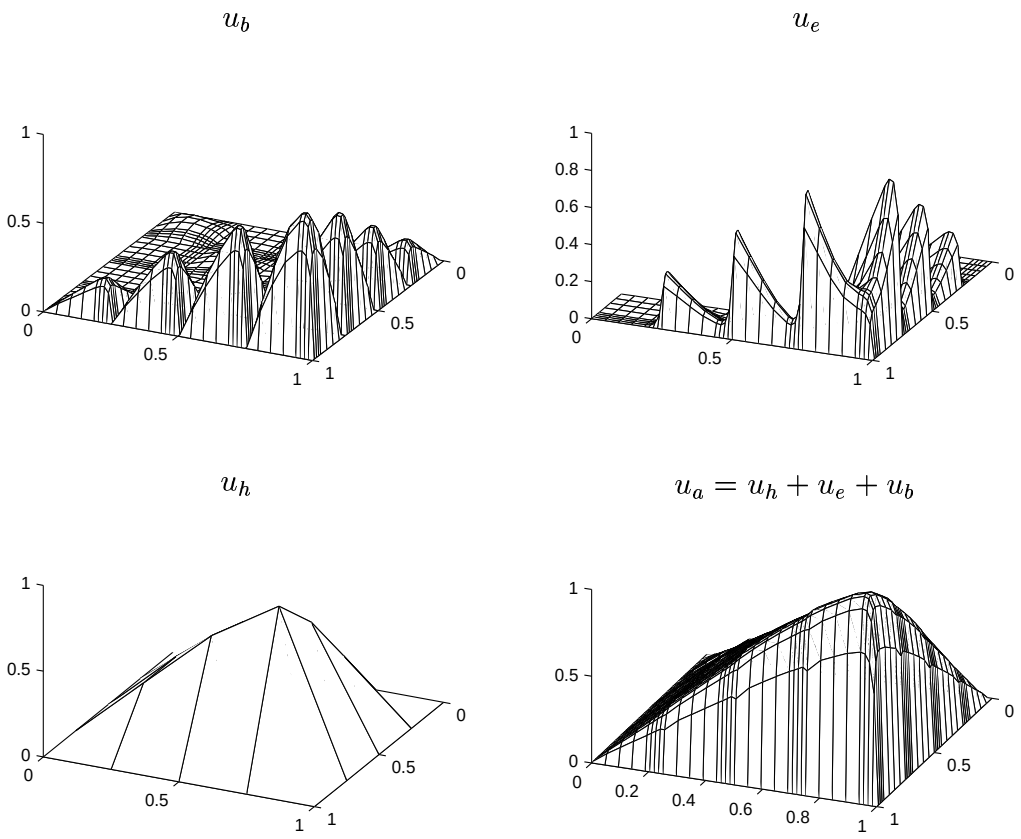

Figure 7: Example 2. The RFBe solution of the boundary value problem (4.5) on a 4×4 uniform mesh for $\varepsilon = 10^{-2}$. The bubbles are computed using a 8×8 Shishkin subgrid.

example), hence the same accuracy in the outside region can be achieved using poorer approximation to the internal bubbles. If we switch off the bubbles in the outside region, we obtain a method similar to the one in [19]; if no other layers are present (as in this example), this yields almost as accurate results as the full RFB method.

Example 2. We solve the boundary value problem with constant coefficients

$$\begin{cases} -\varepsilon \Delta u + \left(\cos(\frac{\pi}{4}), \sin(\frac{\pi}{4})\right) \cdot \nabla u = 1 & \text{in } \Omega = (0,1)^2 \\ u = 0 & \text{on } \partial\Omega. \end{cases} \tag{4.5}$$

In Figure 7 we see the numerical solution obtained by using an RFBe method on a uniform mesh with $h = 1/4$ and $\varepsilon = 10^{-2}$ as a sum of its components in the spaces B_h, E_h and V_h.

The convergence in terms of the mesh parameter h in the $\sqrt{\varepsilon}$-weighted energy norm for $\varepsilon = 10^{-2}$ is shown in Figure 9. As for the subgrid computations, we have used axiparallel Shishkin subgrids with $N = 20$ and $N = 4$ and the Shishkin parameter $c_s = 1/2$.

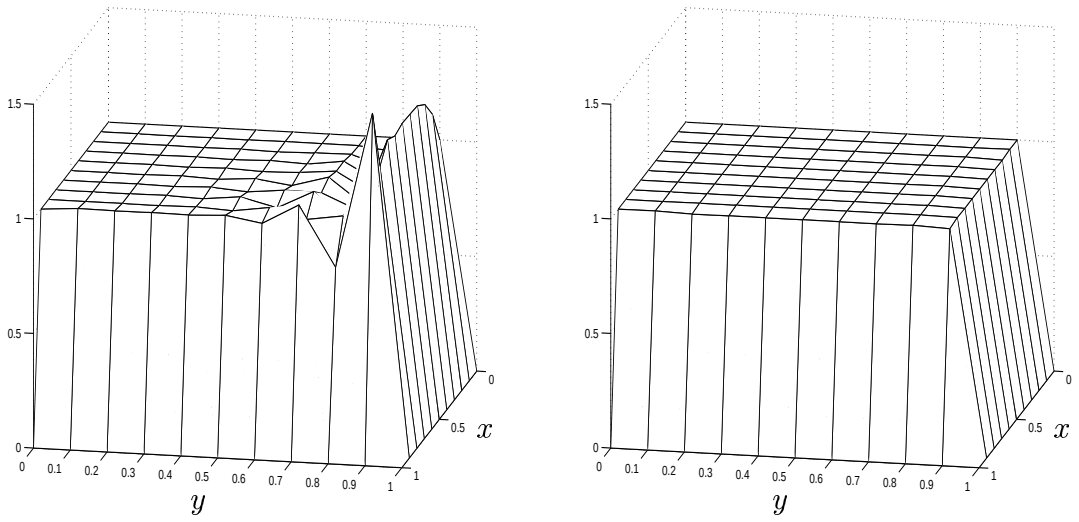

(a) RFB solution

(b) RFBe solution

Figure 8: Solution of Example 4.1in [13]: $f = 0$, $\boldsymbol{a} = (\cos(\pi/6), \sin(\pi/6))$, $\varepsilon = 10^{-7}$ and Dirichlet homogeneous boundary conditions at $x = 1$ and $y = 1$; Dirichlet boundary condition 1 otherwise. The edge bubbles were computed using an 8×8 subgrid.

We notice that, for this problem, the error is almost completely concentrated in the boundary layer, so mesh refinement, particularly in the outside region, is of secondary importance in the regime $h > \varepsilon$.

In contrast with this, as can be seen in Figure 9(b) which reports the error in the outside region $\Omega_{\text{out}} = (0, 1-h)^2$, the accuracy of the RFBe method away from the boundary layer is largely independent from that of the subgrid computations. As long as $\varepsilon < h$, the numerical solutions obtained by using the RFBe method are more accurate than those delivered by the RFB method: the edge bubbles have the effect of eliminating the over– and under–shooting near the boundary layer typical of RFB (and of most stabilised finite element methods). This can be seen by comparing Figures 2 and 7. A similar result was obtained by Mizukami and Hughes [13] with their shock–capturing method which has the additional property of satisfying the discrete maximum principle. Example 4.1 in [13] ($f = 0$, $\boldsymbol{a} = (\cos(\pi/6), \sin(\pi/6))$, $\varepsilon = 10^{-7}$ and homogeneous Dirichlet boundary conditions at $x = 1$ and $y = 1$; Dirichlet boundary condition $u = 1$ otherwise) highlights the problem of over– and under–shooting near the boundary layer. The RFBe solution to this problem is nodally very accurate; see Figure 8.

The energy norm error for different values of ε on a fixed uniform mesh of size $h = 1/8$ is depicted in Figure 10(a). For small values of ε, since we cannot afford to use very fine subgrids, the error due to the approximate computation of the bubbles is dominant. On the other hand, the lower bound on the error given by the error in the outside region, which is largely independent of the subgrid size, permits us to confirm the a-priori bounds (see Figure 10(b)).

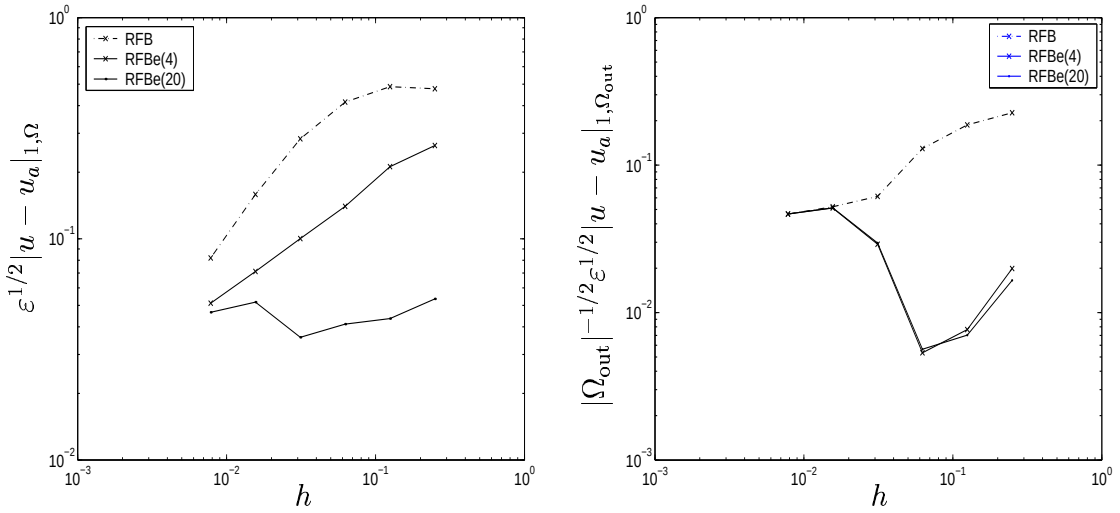

(a) Energy error in Ω (b) Error away from the layers

Figure 9: Example 2. $\sqrt{\varepsilon}$-weighted energy norm error as a function of h.

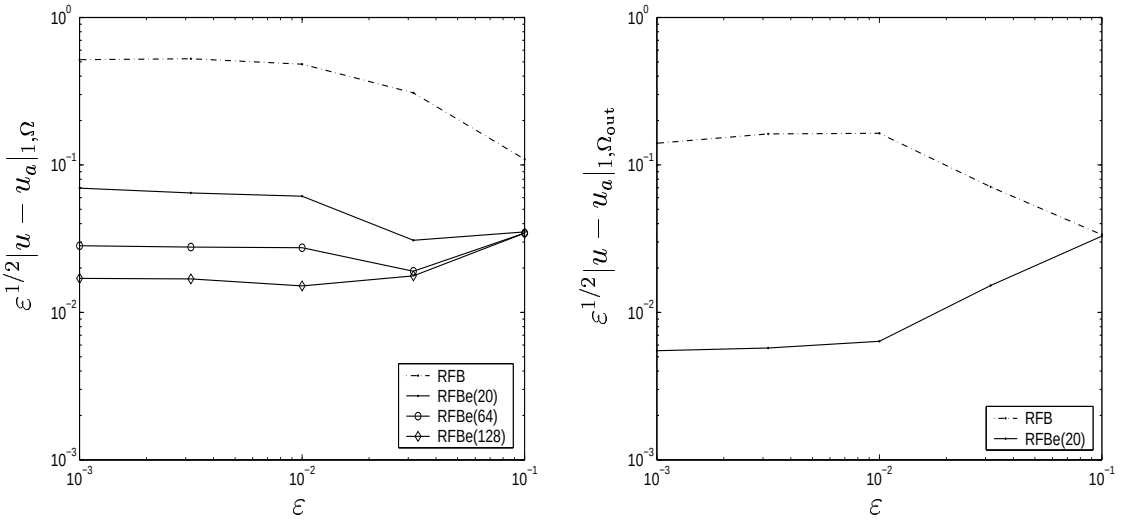

(a) Error vs ε in Ω (b) Error vs ε in $\Omega_{\rm out}$

Figure 10: RFB and RFBe $\sqrt{\varepsilon}$-weighted energy norm error on a uniform mesh of size $h = 1/8$ for different values of ε.

We have verified that the overall accuracy is improved by the introduction of the edge-bubbles. The method achieves both an increased local resolution and a global improvement in accuracy in comparison with RFB (see Figure 9).

In practice, the bases for the bubble spaces must be evaluated numerically by introducing a subgrid. Since the edge-bubbles are not eliminated via static condensation, one may be led to think that the method should be quite sensitive to the accuracy to which the numerical solution is to be computed. In fact, this seems to be true only inasmuch as accuracy within the layer is concerned, as we can see by comparing the plots of Figure 9(a) and (b).

In general, we may not know a-priori where the inclusion of the edge-bubbles is required. Thus, we believe that the RFBe method should be thought of as a corrector in an iteration whose predictor is the RFB method, followed by a loop of a-posteriori error estimation aimed at locating elements where edge bubbles need to be inserted; work in this direction is in progress.

We conclude with an example taken from [6] and with a remark concerning the application of the RFBe method to problems that exhibit internal layers.

Example 3. We solve the boundary value problem considered in [6] using the RFB method:

$$\begin{cases} -\epsilon\Delta u + (\cos(\pi/3), \sin(\pi/3)) \cdot \nabla u = 1 \qquad \text{in } \Omega = (0,1)^2 \\ u = 1 \quad \text{for} \begin{cases} x \le 1/2, y = 0 \\ x = 0 \end{cases} \\ u = 0 \quad \text{otherwise.} \end{cases} \tag{4.6}$$

This problem is not covered by our analysis: because of the presence of an internal layer, the asymptotic approximation we used does not satisfy (3.4). Still, the RFBe results show a considerable improvement over the results obtained by the RFB method.

The solutions obtained by means of the RFB and RFBe methods on a uniform mesh with $h = 1/20$ for $\varepsilon = 10^{-6}$ are shown in Figure 11. We notice that the oscillations near the boundary layer and the spike in the corner layer present in the RFB solution are absent from the RFBe solution. This highlights the fact that such unwanted features of the RFB method are due to poor resolution of the boundary layer on the skeleton of the triangulation.

On the other hand, no visible improvement over the accuracy of RFB is obtained along the internal layer propagating from the point of discontinuity in the boundary condition. One would expect that carefully chosen edge bubbles defined near the layer itself will eliminate this numerical inaccuracy.

5 Conclusions

We have shown how a small number of edge-bubbles can be defined to improve the resolution of boundary layers of the RFB method in the context of convection dominated

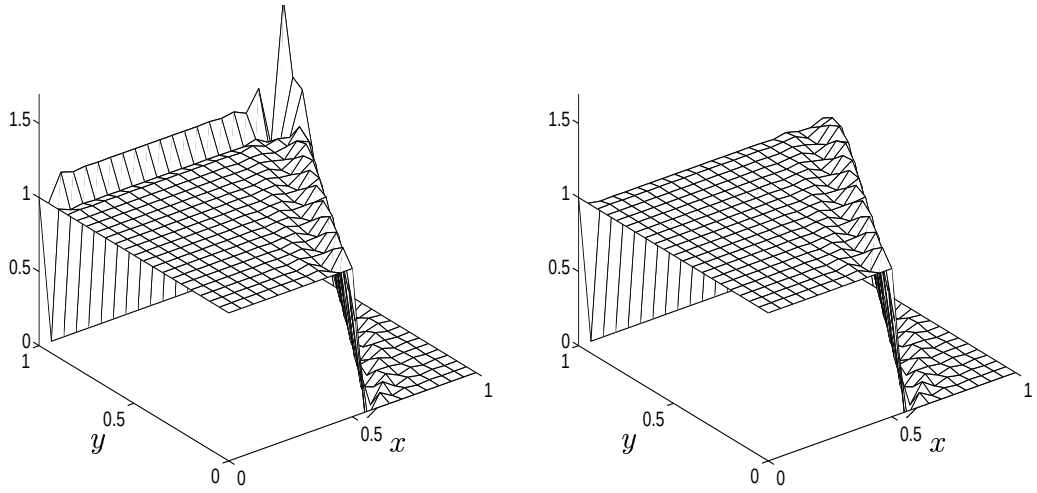

(a) RFB (b) RFBe

Figure 11: Example 3. Solution of a problem with an internal layer on a uniform mesh of size $h = 1/20$. The problem parameters are $\varepsilon = 10^{-6}$, $\boldsymbol{a} = (\cos(\pi/3), \sin(\pi/3))$; as for the subgrid, a Shishkin mesh with $N = 4$ has been used.

convection-diffusion boundary value problems.

The resulting scheme has better accuracy properties then RFB in the regime $\varepsilon < h$. Indeed, both our a-priori error analysis and our numerical experiments show that on coarse meshes the RFB method shows little or no improvement in accuracy in the energy norm, while RFBe exhibits the optimal asymptotic rate of convergence in the energy norm on Ω; in the preasymptotic regime $\varepsilon < h$ standard RFB is only capable of reproducing the same level of accuracy away from the layers.

Moreover, we have noticed that, although we are acting locally, the scheme obtains increased resolution globally, indicating that the introduction of the edge-bubbles has a stabilising effect. More precisely, our method, similarly to the shock-capturing method presented in [13], shows no over- and under-shooting near the boundary-layer. Such improvement is obtained robustly with respect to the subgrid size and hence at (almost) no extra computational work.

Another characteristic feature of RFBe is that accuracy inside the boundary layer region is very sensitive to the accuracy to which the edge-bubbles have been computed; thus, only if high precision on such region is required, should one consider performing expensive and accurate calculations of the edge-bubbles.

Following the ideas of Brezzi and Marini [7], we presented the RFBe method in a general form, suggesting that other multiscale problems for which the fine scale features are only locally present may benefit from the introduction of edge-bubbles. The principle is that we are ready to afford the introduction of only a small number of new degrees of

freedom; hence, for the procedure to work efficiently, we must assume that it is known a-priori where the bubbles have to be added. Such needed information may be obtained from previous computations with, or without the use of a-posteriori error bounds. Work in this direction is in progress.

Acknowledgements

The authors are grateful to Prof. Franco Brezzi for inspiring this paper. This work has greatly benefited from the discussions with Dr. Giancarlo Sangalli which took place at the Newton Institute (Cambridge) during the program '*Computational Challenges in Partial Differential Equations*' (20 January - 4 July 2003). Andrea Cangiani is grateful to the INdAM and to the EPSRC for financial support.

Appendix A Estimates for the asymptotic approximation

Let $u_c = u_{\rm as} - u_0$ be the collection of all correction terms in the asymptotic approximation $u_{\rm as}$ defined by (3.3). We prove that there exists a constant C independent of ε and h such that

$$\sum_{\Gamma\in\Gamma_{\rm out}} |u_c|^2_{1,\Gamma} \le C\frac{{\rm e}^{-2c_0c_ah/\varepsilon}}{\varepsilon^2} \tag{A.1}$$

Let us concentrate on the L_2-norm of the derivative with respect to x (proceeding in a similar way, one can prove a similar bound on the y–derivative). It is sufficient to consider the first term of u_c, i.e.,

$$u_0(1,y){\rm e}^{-a_1(1,y)\frac{1-x}{\varepsilon}}.$$

We start by fixing an edge $\Gamma_{ij} = [x_{i-1}, x_i] \times y_j$. We have:

$$\int_{x_{i-1}}^{x_i} \left| u_0(1,y_j)\frac{\rm d}{{\rm d}x}{\rm e}^{-a_1(1,y_j)\frac{1-x}{\varepsilon}}\right|^2 {\rm d}x \le C\frac{a_1(1,y_j)}{2\varepsilon}\left({\rm e}^{-2a_1(1,y_j)\frac{1-x_i}{\varepsilon}} - {\rm e}^{-2a_1(1,y_j)\frac{1-x_{i-1}}{\varepsilon}}\right).$$

Thus, summing over all edges oriented along the x-axis, we get

$$\begin{aligned}\sum_{j=1}^{n-1}\sum_{i=1}^{m-1}\int_{x_{i-1}}^{x_i} \left| u_0(1,y_j)\frac{\rm d}{{\rm d}x}{\rm e}^{-a_1(1,y_j)\frac{1-x}{\varepsilon}}\right|^2 {\rm d}x &\le C\sum_{j=1}^{n-1}\frac{a_1(1,y_j)}{2\varepsilon}\left({\rm e}^{-2a_1(1,y_j)h_{\rm bl}/\varepsilon} - {\rm e}^{-2a_1(1,y_j)/\varepsilon}\right)\\ &\le C\frac{{\rm e}^{-2c_ah/\varepsilon}}{\varepsilon h},\end{aligned}$$

where $h_{\rm bl} = 1 - x_{M-1}$. Let us now consider the edge $\Gamma_{ji} = x_j \times [y_{i-1}, y_i]$. This time we have

$$\int_{y_{i-1}}^{y_i} \left| u_0(1,y)\left(\frac{\rm d}{{\rm d}x}{\rm e}^{-a_1(1,y)\frac{1-x}{\varepsilon}}\right)_{x=x_j}\right|^2 {\rm d}y \le C\frac{1}{\varepsilon^2}\int_{y_{i-1}}^{y_i} {\rm e}^{-2a_1(1,y)\frac{1-x_j}{\varepsilon}}{\rm d}y \le C\frac{h}{\varepsilon^2}{\rm e}^{-2c_a\frac{1-x_j}{\varepsilon}}.$$

Thus, summing over all edges oriented along the y-axis, we get

$$\begin{aligned}\sum_{j=1}^{m-1}\sum_{i=1}^{n-1}\int_{y_{i-1}}^{y_i}\left|u_0(1,y)\left(\frac{\mathrm{d}}{\mathrm{d}x}\mathrm{e}^{-a_1(1,y)\frac{1-x}{\varepsilon}}\right)_{x=x_j}\right|^2\mathrm{d}y &\leq C\frac{1}{\varepsilon^2}\sum_{j=1}^{m-1}\mathrm{e}^{-2c_a\frac{1-x_j}{\varepsilon}}\\ &\leq C\frac{\mathrm{e}^{-2c_0c_ah/\varepsilon}}{\varepsilon^2}\sum_{j=0}^{m-2}\mathrm{e}^{-2c_0c_a\frac{jh}{\varepsilon}}\\ &\leq C\frac{\mathrm{e}^{-2c_0c_ah/\varepsilon}}{\varepsilon^2}.\end{aligned}$$

A similar argument yields

$$\sum_{\Gamma\in\Gamma_{\mathrm{out}}}||u_c||^2_{0,\Gamma}\leq C\mathrm{e}^{-2c_0c_ah/\varepsilon}. \tag{A.2}$$

As regards the H^1–seminorm of u_c over Γ_{bl}, we show that

$$\sum_{\Gamma\in\Gamma_{\mathrm{bl}}}|u_c|^2_{1,\Gamma}\leq C\frac{1}{\varepsilon h}. \tag{A.3}$$

Let us fix the edge $\Gamma_j=[1-h,1]\times y_j$. The leading term is clearly given by

$$\int_{1-h}^{1}\left|\frac{\mathrm{d}}{\mathrm{d}x}\mathrm{e}^{-a_1(1,y_j)\frac{1-x}{\varepsilon}}\right|^2\mathrm{d}x=\frac{a_1(1,y_j)}{\varepsilon}\left(1-\mathrm{e}^{-a_1(1,y_j)h/\varepsilon}\right)\leq C\frac{1}{\varepsilon},$$

and summing over j, we get (A.3). Again we can proceed in a similar fashion to prove that

$$||u_c||^2_{0,\Gamma}\leq C\varepsilon,$$

and hence

$$\sum_{\Gamma\in\Gamma_{\mathrm{bl}}}||u_c||^2_{0,\Gamma}\leq C\varepsilon h^{-1}. \tag{A.4}$$

Appendix B Shishkin interpolation

Given the one–dimensional boundary value problem

$$\begin{cases}-\varepsilon v_h''+av_h'=f \quad \text{in } I_h=(0,h),\\ v_h(0)=0, \quad v_h(h)=0,\end{cases}$$

we scale it back to the unit interval:

$$\begin{cases}-\varepsilon^* v''+av'=hf \quad \text{in } I=(0,1),\\ v(0)=0, \quad v(h)=0,\end{cases} \tag{B.1}$$

where $\varepsilon^* = \varepsilon/h$, and consider Shishkin interpolation of v.

A Shishkin piecewise equidistant mesh consisting of N subdivisions (with N even) is defined as follows. Given the turning point

$$\lambda^* = c_s(\varepsilon^*/c_a)\ln N,$$

where c_s is a constant independent of ε^* and N, the mesh is taken to be uniform with $N/2$ subdivisions on the two subintervals $(0, 1-\lambda^*)$ and $(1-\lambda^*, 1)$. Thus, the mesh on $[0,1]$ is piecewise uniform. For the continuous piecewise linear interpolant v^I of the solution v of (B.1), the interpolation error over such mesh satisfies (see [15]),

$$\varepsilon^*|v - v^I|^2_{1,I} + ||v - v^I||^2_{0,I} \leq CN^{-2}\ln^2 N,$$

with the constant C independent of ε and N.

Scaling back to the interval I_h we obtain a Shishkin mesh with turning point $\lambda = c(\varepsilon/c_a)\ln N$ and the scaled interpolation error bound

$$\varepsilon|v - v^I|^2_{1,I_h} + h^{-1}||v - v^I||^2_{0,I_h} \leq CN^{-2}\ln^2 N.$$

Shishkin meshes on rectangles are constructed by taking a tensor product of 1-D meshes, and then similar approximation results apply.

References

[1] Adam, D., Felgenhauer, A., Roos, H.-G., and Stynes, M. A nonconforming finite element method for a singularly perturbed boundary value problem. *Computing 54*, 1 (1995), 1–25.

[2] Brezzi, F. Recent results in the treatment of subgrid scales. In *Canum 2000, Actes du 32ème Congrès d'Analyse Numérique*, vol. 11. A. Blouza, I. Danaila, P. Joly, S.M. Kaber, B. Lucquin, F. Murat & M. Postel, Éditeurs ESAIM: Proceedings, 2002, pp. 61–84.

[3] Brezzi, F., Bristeau, M. O., Franca, L. P., Mallet, M., and Rogé, G. A relationship between stabilized finite element methods and the Galerkin method with bubble functions. *Comput. Methods Appl. Mech. Engrg. 96*, 1 (1992), 117–129.

[4] Brezzi, F., Franca, L. P., Hughes, T. J. R., and Russo, A. $b = \int g$. *Comput. Methods Appl. Mech. Engrg. 145*, 3-4 (1997), 329–339.

[5] Brezzi, F., Franca, L. P., Hughes, T. J. R., and Russo, A. Stabilization techniques and subgrid scales capturing. In *The State of the Art in Numerical Analysis (York, 1996)*. Oxford Univ. Press, New York, 1997, pp. 391–406.

[6] Brezzi, F., Franca, L. P., and Russo, A. Further considerations on residual-free bubbles for advective-diffusive equations. *Comput. Methods Appl. Mech. Engrg. 166*, 1-2 (1998), 25–33.

[7] Brezzi, F., and Marini, D. Augmented spaces, two-level methods and stabilising subgrids. In *Numerical methods for fluid dynamics. VII. Proceedings of the Seventh Conference on Computational Fluid Dynamics held at the University of Oxford, Oxford, March 2001*. Ed. Baines, M. J., The Clarendon Press Oxford University Press, New York, 2001.

[8] Brezzi, F., Marini, D., and Süli, E. Residual-free bubbles for advection-diffusion problems: the general error analysis. *Numer. Math. 85*, 1 (2000), 31–47.

[9] Brezzi, F., and Russo, A. Choosing bubbles for advection-diffusion problems. *Math. Models Methods Appl. Sci. 4*, 4 (1994), 571–587.

[10] Eckhaus, W. *Asymptotic analysis of singular perturbations*, vol. 9 of *Studies in Mathematics and its Applications*. North-Holland Publishing Co., Amsterdam, 1979.

[11] Hou, T. Y., and Wu, X.-H. A multiscale finite element method for elliptic problems in composite materials and porous media. *J. Comput. Phys. 134*, 1 (1997), 169–189.

[12] Hou, T. Y., Wu, X.-H., and Cai, Z. Convergence of a multiscale finite element method for elliptic problems with rapidly oscillating coefficients. *Math. Comp. 68*, 227 (1999), 913–943.

[13] Mizukami, A., and Hughes, T. J. R. A Petrov-Galerkin finite element method for convection-dominated flows: an accurate upwinding technique for satisfying the maximum principle. *Comput. Methods Appl. Mech. Engrg. 50*, 2 (1985), 181–193.

[14] O'Riordan, E., and Stynes, M. A globally uniformly convergent finite element method for a singularly perturbed elliptic problem in two dimensions. *Math. Comp. 57*, 195 (1991), 47–62.

[15] Roos, H.-G., Stynes, M., and Tobiska, L. *Numerical Methods for Singularly Perturbed Differential Equations.* Springer-Verlag, Berlin, 1996. Convection-diffusion and flow problems.

[16] Sangalli, G. Global and local error analysis for the residual–free bubbles method applied to advection–dominated problems. *SIAM J. Numer. Anal. 38*, 5 (2000), 1496–1522 (electronic).

[17] Sangalli, G. Capturing small scales in elliptic problems using a residual–free bubbles finite element method. *Multiscale Modeling and Simulation: A SIAM Interdisciplinary Journal 1*, 3 (2003), 485–503.

[18] Schieweck, F. *Eine asymptotisch angepaßte Finite–Element–Methode für singulär gestörte elliptische Randwertaufgaben.* Dissertation, TH Magdeburg, 1986.

[19] Schieweck, F. Numerische integration bei der finite-element-diskretisierung singulär gestörten elliptischer randwertaufgaben. *Wiss. Z. Techn. Universität Magdeburg* (1987).